Review Article

Solar Fuels

COF-Based S-Scheme Photocatalysts for CO2 Conversion: Interfacial Charge Migration and Molecular Activation

Feifan Zhao[1], Xianluo Hu[1], Jianjun Zhang[2], Diego Mateo[3], Alireza Z. Moshfegh[4], Jahan B. Ghasemi[5], Feiyan Xu[2*]

[1] School of Materials Science and Engineering, Huazhong University of Science and Technology, Wuhan 430074, P. R. China
[2] Laboratory of Solar Fuel, Faculty of Materials Science and Chemistry, China University of Geosciences, Wuhan 430078, P. R. China
[3] Instituto Universitario de Tecnología Química, CSIC-UPV, Universitat Politècnica de València, Valencia 46022, Spain
[4] Department of Physics, Sharif University of Technology, Tehran 11555-9161, Iran
[5] Chemistry Faculty, School of Sciences, University of Tehran, Tehran, Iran

Abstract

Solar-driven photocatalytic CO_2 conversion offers a sustainable route for coupling carbon recycling with solar-to-chemical energy storage. However, its efficiency and product selectivity are limited by rapid charge recombination, inefficient CO_2 enrichment and activation, competing proton reduction, and poorly controlled electron/proton transfer during multistep conversion. Covalent organic framework (COF)-based step-scheme (S-scheme) heterojunctions provide a distinctive platform in which selective interfacial recombination can promote charge separation while preserving strongly reducing electrons and oxidizing holes. Meanwhile, the molecular programmability of COFs enables the regulation of interfacial coupling, catalytic sites, and pore microenvironments to facilitate CO_2 enrichment and activation and control reaction pathways. This Review examines how COF-based S-scheme interfaces are constructed, how their charge-transfer pathways can be reliably established, and how interfacial charge migration translates into productive CO_2 chemistry. Particular attention is paid to interfacial bonding, charge redistribution, built-in electric-field formation, photoinduced carrier migration, and their relationships with intermediate stabilization and multielectron reduction. A central conclusion is that charge separation and catalytic charge utilization are distinct but inseparable design challenges. Future advances will require chemically well-defined interfaces, operando and time-resolved mechanistic validation, and the reaction-specific integration of charge migration, active-site chemistry, proton transfer, and pore microenvironments.

Keywords: covalent organic frameworks, S-scheme heterojunctions, interfacial coupling, interfacial charge transfer, CO_2 activation, proton-coupled electron transfer

Introduction

The increasing atmospheric concentration of CO_2, driven largely by intensive fossil-resource consumption, has stimulated considerable interest in technologies that can close the anthropogenic carbon cycle [1,2]. Photocatalytic CO_2 conversion offers an attractive route for coupling solar-energy utilisation with carbon recycling by transforming CO_2 into fuels and value-added chemicals, including CO, CH_4, CH_3OH, and multicarbon products [3,4]. However, its practical realisation is hindered by several coupled physicochemical limitations. The linear geometry and strong C=O bonds of CO_2 make its polarisation and initial activation energetically demanding, while insufficient local enrichment or unproductive adsorption can further restrict surface conversion [5,6]. Rapid bulk and interfacial recombination also leaves only a fraction of the photogenerated carriers available for catalytic reactions. Moreover, CO_2 reduction generally proceeds through sequential multielectron and proton-coupled electron-transfer steps; therefore, product formation depends critically on how reaction intermediates are generated, stabilised, and further transformed. Insufficient intermediate stabilisation can terminate reduction prematurely, whereas overly strong binding may impede subsequent conversion or product desorption [7,8]. In proton-containing media, hydrogen evolution further competes with CO_2 reduction for photogenerated electrons, particularly when CO_2 activation is

Received: September 29, 2026; Revised: October 7, 2026
Accepted: October 8, 2026; Published Online: November 3, 2026
*Corresponding author: E-mail: xufeiyan@cug.edu.cn
DOI: 10.68642/fuel.202600003

Check for updates

DOI: 10.68642/fuel.202600003

inefficient or electron delivery to CO_2-derived intermediates is kinetically unfavourable [9]. Therefore, effective CO_2 photoconversion requires not only efficient charge separation but also the preservation of sufficient redox driving force and selective delivery of carriers to catalytic sites that can direct the desired reaction pathway.

Heterojunction engineering is a widely used strategy for manipulating photogenerated charge carriers. Traditional type-II heterojunctions can promote spatial charge separation, but the associated downhill carrier transfer generally sacrifices part of the redox energy available after separation [10,11]. Step-scheme (S-scheme) heterojunctions are attractive in this context because they seek to combine efficient carrier separation with the retention of strongly reducing electrons and strongly oxidising holes [12,13]. However, for CO_2 conversion, retaining energetic carriers addresses only the photophysical part of the problem. Their catalytic value ultimately depends on whether these carriers reach appropriate reaction sites and are productively coupled to proton transfer and intermediate evolution [11,14,15]. Thus, S-scheme design can improve carrier availability and redox competence, but it does not by itself determine how those carriers are chemically utilised.

Covalent organic frameworks (COFs) offer a molecularly programmable platform for bridging these photophysical and catalytic requirements. Their π-conjugated skeletons, modular building units, and tunable electronic structures enable systematic regulation of light absorption, band energetics, and charge distribution [16–20]. Meanwhile, heteroatoms and coordination motifs embedded within COF backbones provide chemically addressable sites for coupling semiconductors, molecular catalytic units, and other functional components through noncovalent interactions, coordination bonds, or covalent linkages. Owing to this structural versatility, the interface itself can be tuned in terms of bonding configuration, electronic coupling, and local catalytic environment, rather than serving merely as a physical contact between two photoactive components [21–24]. The ordered porosity of COFs further provides opportunities to regulate local CO_2 concentration, reactant transport, proton accessibility, and exposure of active sites [25–27]. Consequently, COF-based S-scheme heterojunctions provide a framework in which charge migration, molecular activation, and the reaction microenvironment can be engineered in a coordinated manner.

Despite rapid progress in COF-based S-scheme photocatalysts, substantial uncertainty remains regarding how interfacial structure, charge-transfer pathways, and CO_2 reaction chemistry are causally connected. Recent reviews have summarised advances in materials construction, heterojunction configurations, charge-transfer concepts, and photocatalytic applications [16,17,27]. Building on these efforts, the present Review focuses more specifically on two interconnected questions: how S-scheme charge-transfer pathways can be reliably established through discriminating evidence and how the retained carriers are subsequently utilised in CO_2 activation, intermediate evolution, and product-selective conversion. Band alignment, X-ray photoelectron spectroscopy (XPS) shifts, radical trapping, and enhanced catalytic activity are often used individually to support S-scheme assignments, although none of these observations alone establishes the complete charge-transfer mechanism. More importantly, improved charge separation does not necessarily imply the productive utilisation of the retained carriers in CO_2 activation or selective intermediate conversion. Accordingly, this Review examines the interfacial physics and coupling modes of COF-based S-scheme heterojunctions, critically evaluates the evidence required to establish their charge-transfer pathways, and connects interfacial carrier behaviour with CO_2 enrichment, molecular activation, intermediate evolution, and product selectivity. Particular emphasis is placed on distinguishing energetic feasibility from mechanistic proof and carrier separation from productive charge utilisation, thereby providing a framework for the reaction-specific design of COF-based S-scheme photocatalysts.

Interfacial Physics of COF-Based S-Scheme Heterojunctions

From conventional heterojunctions to S-scheme charge transfer

Early heterojunction design primarily aimed to suppress electron–hole recombination through spatial charge separation. Traditional type-II heterojunctions are typically described by a staggered band alignment, in which photogenerated electrons migrate from the higher-lying conduction band (CB) to the lower-lying CB, while holes migrate towards the valence band (VB) with weaker oxidation capability. Although this classical picture provides an intuitive route to spatially separate electrons and holes, it has several limitations. First, the energetically downhill migration dissipates part of the free energy of the photogenerated carriers, leaving electrons and holes with weaker reduction and oxidation capabilities, respectively, and thereby restricting thermodynamically demanding surface reactions. Second, in particulate photocatalytic systems, progressive charge accumulation on the receiving components modifies the interfacial electrostatic potential and can oppose further transfer, making carrier migration more complex than predicted solely from the relative band positions of the isolated semiconductors. Third, semiconductor contact itself can induce Fermi-level equilibration, interfacial charge redistribution, and band bending; hence, the electronic structure of the equilibrated heterointerface cannot be fully represented by a simple pre-contact band-offset diagram. Consequently, the traditional type-II model faces a fundamental difficulty in simultaneously accounting for efficient charge separation, the preservation of strong redox capability, and the actual carrier-transfer pathway at a contacted photocatalytic interface [28–31].

Z-scheme photocatalytic systems were developed to preserve strongly reducing electrons and strongly oxidising holes rather than allowing both carrier populations to relax towards the less energetic states expected in a type-II pathway. Early liquid-phase Z-schemes employed reversible redox couples to mediate charge transfer between physically separated reduction and oxidation photocatalysts. Although this configuration was designed to retain high-energy carriers, it relies on mediator diffusion and

DOI: 10.68642/fuel.202600003

redox cycling and can be complicated by reverse reactions, mass-transfer limitations, and competing redox processes [32,33]. All-solid-state Z-schemes subsequently replaced soluble mediators with solid electron conductors, which provided a fixed charge-transfer pathway but introduced an additional component and multiple interfaces whose spatial arrangement, contact quality, and electronic properties influence charge transport. Direct Z-scheme heterojunctions further eliminated the external mediator by bringing the two photocatalysts into intimate contact, thereby simplifying the architecture while retaining the central objective of preserving carriers with strong reduction and oxidation capabilities [34–36].

The development of liquid-phase, all-solid-state, and direct Z-scheme architectures broadened the Z-scheme concept but also made it harder to identify the underlying charge-transfer pathways consistently, because systems with substantially different physical structures were described within the same general framework. The S-scheme concept, introduced in 2019 for directly coupled photocatalysts, describes such charge transfer more explicitly in terms of interfacial physics. The two components are designated as a reduction photocatalyst (RP) and an oxidation photocatalyst (OP), and their work-function and Fermi-level differences, contact-induced charge redistribution, band bending, and internal electric field (IEF) are explicitly considered when describing photoinduced carrier migration. Viewed in this way, the progression from traditional type-II and mediator-assisted Z-scheme systems to direct-contact and S-scheme descriptions reflects two intertwined developments: the pursuit of efficient charge separation without sacrificing redox power, and the increasing emphasis on the post-contact interfacial electronic structure in describing selective carrier migration [11,37,38]. This historical progression is summarised in Figure 1.

Interfacial formation and photoinduced charge migration in S-scheme heterojunctions

In the canonical S-scheme model, the interfacial energetic landscape is established before illumination. Before contact, the RP typically possesses a higher Fermi level and a lower work function than the OP. Once an intimate interface is formed, electrons spontaneously diffuse from the RP to the OP until Fermi-level equilibration is reached. The resulting electron depletion on the RP side and electron accumulation on the OP side generate oppositely charged interfacial regions. This contact-induced redistribution produces upward band bending in the RP and downward band bending in the OP, as well as an IEF directed from the positively charged RP towards the negatively charged OP. Together, Fermi-level equilibration, interfacial charge redistribution, band bending, and IEF formation define the equilibrium electronic structure of the S-scheme interface. These features describe the ground-state interfacial landscape established upon contact and provide the energetic basis for the subsequent migration of photogenerated carriers [11,30].

Upon photoexcitation, the pre-established band bending and IEF bias the migration of photogenerated carriers across the interface. In the canonical S-scheme description, photogenerated electrons with relatively weak reduction capability in the OP migrate towards the interface and recombine with holes of relatively weak oxidation capability in the RP. In contrast, the strongly reducing electrons in the RP and strongly oxidising holes in the OP are retained for subsequent reduction and oxidation reactions, respectively. Therefore, the key consequence is the selective removal of carriers with weaker redox capability and the spatial retention of strongly reducing electrons and strongly oxidising holes. These processes are summarised schematically in Figure 2.

However, for COF-containing heterointerfaces, this canonical S-scheme description should be applied with caution. The degree of carrier delocalisation, interfacial electronic coupling, and structural order can differ substantially from those in conventional inorganic semiconductor junctions. Accordingly, contact-induced charge redistribution, local potential gradients, band bending, and IEF formation should be established experimentally rather than inferred solely from schematic band align-

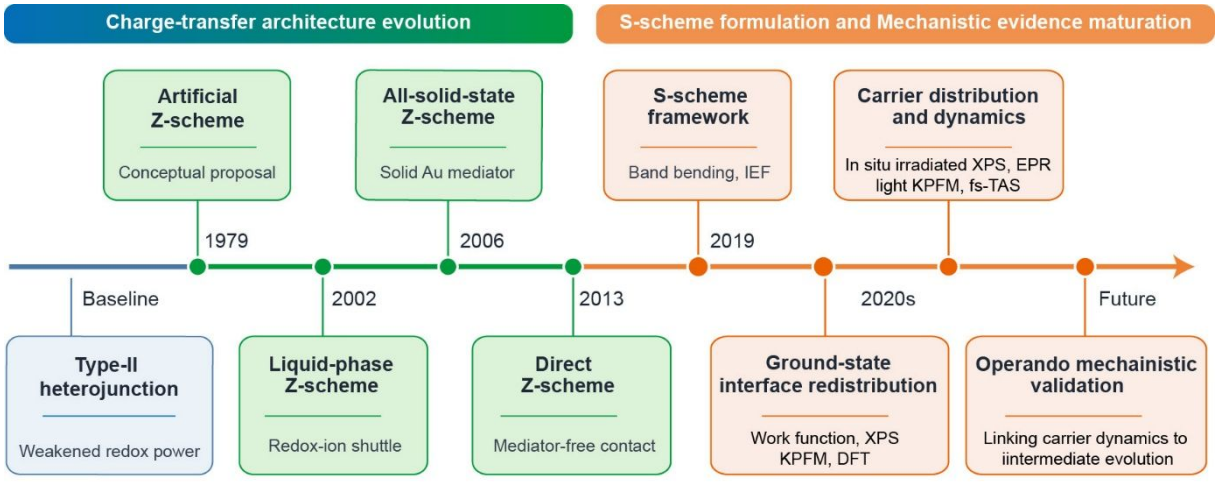


Fig. 1 Evolution of charge-transfer architectures and mechanistic validation in step-scheme photocatalysis. Conceptual schematic based on Refs. [11,33–37]. DFT, density functional theory; EPR, electron paramagnetic resonance; fs-TAS, femtosecond transient absorption spectroscopy; IEF, internal electric field; KPFM, Kelvin probe force microscopy; XPS, X-ray photoelectron spectroscopy.

DOI: 10.68642/fuel.202600003

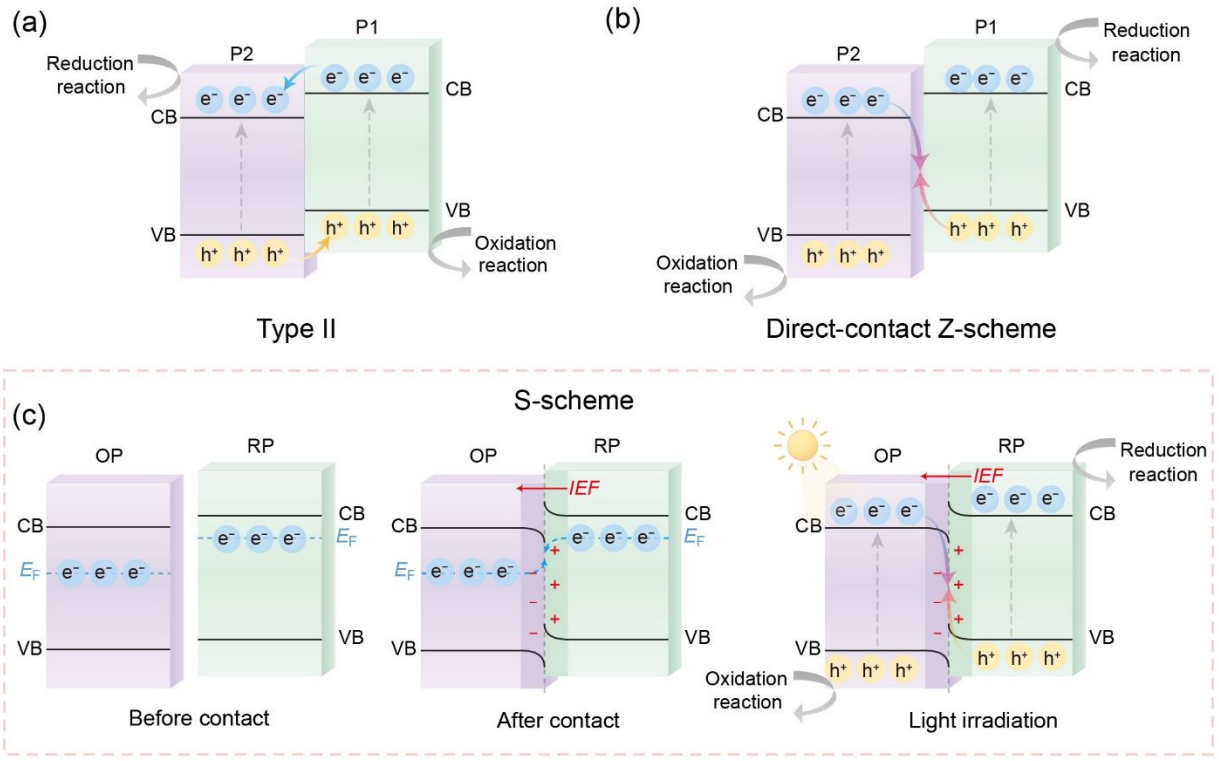


Fig. 2 Schematic comparison of energetic alignment, interfacial charge redistribution, and photoinduced carrier migration in (a) traditional type-II, (b) direct-contact Z-scheme, and (c) step-scheme heterojunctions. Conceptual schematic based on Refs [11,30].

ment. Likewise, the direction of photoinduced carrier transfer requires independent light-dependent or time-resolved evidence. This distinction is particularly important when assigning an S-scheme mechanism and forms the basis for the evidence hierarchy discussed later in this Review [39–41].

Therefore, for photocatalytic CO_2 conversion, the S-scheme framework identifies which photogenerated carriers remain energetically available for interfacial redox chemistry, whereas their subsequent delivery to and utilisation at catalytic sites depend strongly on the chemical structure and electronic coupling of the COF interface. This relationship provides the basis for discussing the noncovalent, coordination-mediated, and covalent coupling modes in the following section [42,43].

Interfacial Coupling Modes in COF-Based S-Scheme Heterojunctions

The interfacial energetic landscape described above provides the driving force for S-scheme charge migration, but it does not alone determine how efficiently photogenerated carriers cross a real heterointerface. Interfacial distance, bonding configuration, orbital overlap, and electronic coupling can all influence the kinetics and directionality of charge transfer. This issue is particularly important for COF-based heterojunctions because the modular backbones and chemically addressable functional groups of COFs enable the interface to be engineered at the molecular level. Therefore, different coupling modes can alter not only structural contact and interfacial stability but also local charge redistribution and electronic communication between the coupled components.

Based on the dominant interfacial interaction, COF-based S-scheme heterojunctions can be broadly classified into noncovalently assembled, coordination-mediated, and covalently bridged interfaces. These categories are not necessarily mutually exclusive, because multiple interactions may coexist at a practical heterointerface. Nevertheless, they provide a useful framework for examining how interfacial chemistry governs electronic coupling and charge-transfer behaviour.

Noncovalently assembled interfaces

Noncovalently assembled interfaces couple photocatalytic components through van der Waals forces, π–π interactions, electrostatic attraction, hydrogen bonding, or combinations thereof. Their principal advantages include synthetic simplicity, mild assembly conditions, broad materials compatibility, and minimal perturbation of the intrinsic structures of the individual components. These characteristics make noncovalent assembly particularly suitable for two-dimensional COFs, layered semiconductors, and other extended π-conjugated materials, for which large-area interfacial contact can be established without forming new chemical bonds [44–47].

A representative example is the defective g-C_3N_4(NH)/Tp-Tta COF van der Waals S-scheme heterojunction prepared by solvent-evaporation-induced self-assembly. The face-to-face contact enlarged the effective interfacial area, while N vacancies

DOI: 10.68642/fuel.202600003

in g-C_3N_4 increased the energetic asymmetry between the two components and promoted interfacial charge redistribution. Density functional theory (DFT) calculations and electron paramagnetic resonance (EPR) measurements further supported appreciable electronic communication across the van der Waals interface, illustrating that efficient interfacial charge transfer does not necessarily require covalent bonding. A related strategy was demonstrated by coupling photoreduced graphene oxide with an sp^2-carbon-linked TP-COF through electrostatic self-assembly, with π–π interactions further stabilising the contact between the conjugated components. The resulting interface supported S-scheme charge migration while retaining strongly reducing electrons on the COF component for CO_2-to-CO conversion [48,49].

The electronic behaviour of a noncovalent interface is also highly sensitive to the contact configuration of the two components. This effect is illustrated by Tp-Tta COF/TiO_2 heterojunctions constructed with different exposed TiO_2 facets. The T-101/COF system exhibited a CO_2 reduction rate of 11.6 μmol h^{-1}, approximately 4.6 times that of T-001/COF, indicating that interfacial orientation and the associated local electronic structure can substantially influence carrier migration even when the overall chemical compositions are similar. Therefore, noncovalent interfaces should not be viewed simply as weakly coupled contacts. Their effectiveness depends on interfacial distance, contact area, orientation, structural complementarity, and local electrostatics. At the same time, the absence of site-specific chemical anchoring can lead to heterogeneous contact, less precisely defined electronic coupling, and possible structural rearrangement during prolonged photocatalysis. Direct correlations between these structural parameters and quantitative charge-transfer kinetics remain comparatively scarce for COF-based S-scheme systems [50]. Representative noncovalently assembled COF-based S-scheme heterojunctions are summarised in Table 1.

Coordination-mediated interfaces

Coordination-mediated interfaces exploit heteroatom-containing sites in COFs to establish metal–ligand interactions with the coupled component. Nitrogen-, oxygen-, and sulfur-containing functionalities can coordinate interfacial metal centres through M–N, M–O, or M–S interactions, providing site-specific anchoring without direct covalent fusion of the two components. Compared with purely noncovalent assembly, coordination can generate a more chemically defined local interface while simultaneously modifying the electronic structures of the interacting sites. Therefore, orbital interactions across the coordination bond can provide a pathway for both ground-state charge redistribution and photoinduced electronic communication [56,57].

This role is exemplified by a ZnO/imine-linked COF S-scheme heterojunction in which X-ray absorption spectroscopy (XAS), XPS, and theoretical calculations identified interfacial Zn–N coordination. The Zn–N linkage provided a chemically defined pathway for electronic communication between ZnO and the COF, while femtosecond transient absorption spectroscopy (fs-TAS) revealed rapid interfacial carrier transfer. Similar behaviour was observed in a WO_3/COF heterojunction, where interfacial N–W coordination was associated with directional S-scheme charge migration. Light-dependent XPS, X-ray absorption near-edge structure (XANES), and ultrafast spectroscopy collectively connected the chemically defined interfacial bond with changes in electronic structure and carrier dynamics [58,59].

Coordination can also reshape the interfacial energetic landscape before photoexcitation rather than act solely as a transfer bridge. In a TPT-COF/ZnO system for photocatalytic CO_2 reduction, interfacial Zn–N donor–acceptor coordination induced local electronic redistribution in the dark state and, together with Fermi-level equilibration, increased the interfacial energetic asymmetry and strengthened the IEF. The resulting interfacial preorganisation accelerated subsequent photoinduced S-scheme charge migration and favoured selective CO_2-to-CH_4 conversion. This example highlights an important feature of coordination-mediated interfaces: a coordination bond can simultaneously regulate local orbital interactions and the broader electrostatic environment of the heterointerface [60].

Therefore, the principal advantage of coordination-mediated

Table 1 Representative noncovalently assembled COF-based S-scheme photocatalysts.

Photocatalyst	Interfacial interaction	Effect on interfacial electronic structure and charge transfer	Ref.
g-C_3N_4(NH)/Tp-Tta COF	van der Waals interaction	Enhanced charge redistribution and interfacial transfer	[48]
TiO_2/Tp-Tta COF	van der Waals interaction	Contact-dependent charge transfer	[50]
PRGO/TP-COF	Electrostatic interaction; π–π interaction	Improved interfacial electronic communication	[49]
3D COF/ZnSe QDs	Hydrogen-bond-assisted anchoring	Improved contact and interfacial charge separation	[51]
TpPa-1-COF/g-C_3N_4	π–π conjugated interaction	Stronger charge redistribution and IEF	[52]
ZnO/TpPa-Cl COF	Electrostatic interaction	Facilitated interfacial carrier transfer	[53]
CdS/TpBD COF	Electrostatic interaction	Shortened interfacial transfer distance	[54]
ZnSe QDs/Ta-Dva COF	Electrostatic interaction	Rapid carrier separation and spatial transfer	[55]

3D, three-dimensional; COF, covalent organic framework; IEF, internal electric field; PRGO, photoreduced graphene oxide; QDs, quantum dots; S-scheme, step-scheme.

coupling lies in its ability to establish site-specific relationships among interfacial structure, local electronic states, and carrier migration. However, its effectiveness cannot be inferred from the presence of a coordination bond alone. Coordination geometry, bond strength, orbital symmetry and energy matching, metal oxidation state, and the surrounding chemical environment can all determine whether a particular linkage facilitates productive electronic communication. Therefore, coordination chemistry should be regarded as a means of programming interfacial electronic coupling rather than of simply strengthening structural contact [63–66]. Representative coordination-mediated systems and their interfacial linkages are summarised in Table 2.

Covalently bridged interfaces

Covalently bridged interfaces chemically connect the COF with another photocatalytic component through direct bond formation between complementary functional groups. Representative linkages include C–N, C–S, imine-derived bridges, and other covalent connections formed during post-synthetic coupling or *in situ* growth. Such interfaces are generally structurally robust and provide short, chemically defined pathways for electronic communication. When the bonding geometry and orbital energetics are favourable, covalent bridging can enhance orbital overlap and facilitate interfacial charge transfer.

Mu *et al.* demonstrated this strategy in an N–ZnO/TAPT-DMTP COF heterojunction for photocatalytic CO_2 reduction [43]. An interfacial Schiff-base reaction covalently linked amino-functionalised ZnO to the COF through an imine bridge. Compared with a noncovalently contacted ZnO/COF counterpart, the covalently connected heterostructure exhibited more efficient migration and separation of photogenerated charges. Importantly, operando characterisation and theoretical calculations further connected interfacial charge redistribution with reaction energetics: directional electron accumulation on the COF component lowered the free-energy requirement for the key *COOH-to-*CO conversion step. Therefore, the covalent interface influenced not only carrier transport but also the subsequent chemical utilisation of the redistributed charges.

Direct chemical bridging has also been demonstrated through C–S linkages. In a COF@Co_9S_8 S-scheme heterojunction, C–S bonds generated during *in situ* growth established intimate chemical contact between the two components and facilitated the transfer and separation of photogenerated carriers. These examples illustrate the potential of covalent integration to reduce structural ambiguity at the interface and to connect electronic communication more directly with specific bonding motifs [67].

Nevertheless, covalent integration introduces important trade-offs. Forming new interfacial bonds often requires more elaborate synthetic procedures and can disrupt COF crystallinity, modify local conjugation, or perturb the intrinsic electronic structures of the coupled components. Strong chemical integration may also reduce the freedom to optimise each component independently and, in some cases, alter or block catalytically accessible sites. Covalent interface engineering should therefore aim not at maximising bond strength but at achieving an appropriate balance among structural robustness, orbital coupling, energetic matching, charge-transfer kinetics, and accessibility of functional sites [68–71]. Representative covalently bridged systems are summarised in Table 3.

Across these coupling modes, bonding strength alone does not determine S-scheme performance. Noncovalent interfaces can support rapid charge transfer when intimate contact and favourable electronic coupling are achieved, whereas coordination and covalent bonds can provide more site-specific pathways but may also perturb the intrinsic electronic structures of the constituent materials. Therefore, the relevant design question is whether a given interface establishes appropriate energetic asymmetry, effective electronic communication, and a well-defined pathway for directional charge redistribution and photoinduced carrier transfer. Demonstrating that these processes actually occur requires evidence beyond structural identification of the interface, as discussed in the following section. Table 4 compares the distinguishing features, advantages, and limitations of the three coupling modes.

Establishing S-Scheme Charge Transfer: Mechanistic Evidence and Pitfalls

Establishing an S-scheme mechanism in COF-based heterojunctions requires more than demonstrating favourable band alignment or enhanced charge separation. Traditional type-II and S-

Table 2 **Representative coordination-mediated COF-based S-scheme photocatalysts.**

Photocatalyst	Interfacial interaction	Evidence for interfacial connection	Effect on interfacial electronic structure and charge transfer
TPT-COF/ZnO QDs [60]	Zn–N	FTIR; EXAFS	Local charge redistribution; enhanced interfacial driving force
ZnO/COF [58]	Zn–N	XAS; XPS; DFT	Chemically defined charge-transfer pathway
COF/CdS [61]	Cd–N/Cd–S	XAS; XPS; DFT	Defined interfacial transfer channels
WO_3/COF [59]	N–W	XANES; XPS	Ultrafast directional electron transfer
COF/$ZnIn_2S_4$ [62]	Zn–O	XAFS; DFT	Anchored interfacial state; strengthened IEF

COF, covalent organic framework; DFT, density functional theory; EXAFS, extended X-ray absorption fine structure; FTIR, Fourier transform infrared spectroscopy; IEF, internal electric field; QDs, quantum dots; S-scheme, step-scheme; XAFS, X-ray absorption fine structure; XANES, X-ray absorption near-edge structure; XAS, X-ray absorption spectroscopy; XPS, X-ray photoelectron spectroscopy.

DOI: 10.68642/fuel.202600003

Table 3 Representative covalently bridged COF-based S-scheme photocatalysts.

Photocatalyst	Interfacial interaction	Evidence for interfacial connection	Effect on interfacial electronic structure and charge transfer
N-ZnO/TAPT-DMTP COF [43]	C=N	FTIR; XPS	Stronger electronic coupling and directional transfer
APTES–Cu_2O/COF [68]	APTES-mediated covalent bridge	FTIR; solid-state ^{13}C NMR; DFT	Enhanced interfacial charge transport
Sb_2S_3@COF-LC [69]	Sb–O–C bridge	XPS	Enhanced charge transfer and space-charge separation
Zr-BTB-NH_2/TpTt-COF [70]	β-Ketoenamine bridge	FTIR	Strengthened interfacial electronic coupling and IEF
COF@Co_9S_8 [67]	C–S	XPS	Direct carrier-transfer pathway
D@A-COF [72]	C=N	FTIR; XPS	Continuous interfacial electronic pathway
SnS_2/TaTp-COF [71]	C–N–S	DFT (ELF, PDOS)	Hybrid interfacial states; stronger electronic coupling

APTES, (3-aminopropyl)triethoxysilane; COF, covalent organic framework; DFT, density functional theory; ELF, electron localisation function; FTIR, Fourier transform infrared spectroscopy; IEF, internal electric field; NMR, nuclear magnetic resonance; PDOS, projected density of states; S-scheme, step-scheme; XPS, X-ray photoelectron spectroscopy.

Table 4 Comparison of interfacial coupling modes in COF-based S-scheme heterojunctions.

Interface mode	Dominant interaction/bonding	Structural definition	Electronic coupling	Interfacial robustness	Main advantage	Typical limitation
Noncovalent	van der Waals interaction, π–π, electrostatic interaction, H-bonding	Relatively poorly defined; highly contact-dependent	Variable and often spatially heterogeneous	Moderate; sensitive to contact configuration and possible reconstruction	Facile fabrication; mild conditions; broad materials compatibility; limited perturbation of the parent components	Heterogeneous coupling; contact-dependent charge-transfer kinetics; local interface difficult to define precisely
Coordination-mediated	M–N, M–O, M–S	More site-specific when the coordination motif is identified, but local coordination environments may remain heterogeneous	Orbital-mediated and potentially directional	Generally improved but strongly dependent on the coordination environment	Site-specific anchoring; local electronic-structure regulation; chemically defined electronic communication	Sensitive to coordination geometry and orbital matching; multiple coordination environments may coexist
Covalent	C=N, C–N, C–S, M–O–C	Relatively well-defined when bond formation is directly established	Potentially strong and continuous	Generally high	Robust structural connection; well-defined electronic pathway; potentially reduced interfacial resistance	Higher synthetic complexity; possible perturbation of COF crystallinity/conjugation; reduced independent tunability of components

COF, covalent organic framework; M, metal; S-scheme, step-scheme.

scheme configurations may share similar pre-contact energy-level arrangements, and COFs themselves introduce additional complexity through molecularly defined frontier orbitals, excitonic states, intraframework donor–acceptor charge transfer, chemically heterogeneous interfaces, and porous architectures. Signals commonly attributed to interfacial S-scheme transfer may therefore also arise from intrinsic COF photophysics, local coordination or covalent bonding, defect trapping, or changes in the reaction microenvironment. Consequently, a convincing mechanistic assignment must connect three distinct stages: energetic feasibility before contact, electronic reconstruction of the interface in the ground state, and carrier distribution and

dynamics after photoexcitation. It is equally important to determine whether the observed response is genuinely interfacial or can be explained by changes intrinsic to the COF itself.

Band alignment and energetic prerequisites

The first requirement for an S-scheme assignment is an energetically viable configuration. The electrons and holes proposed to remain after selective interfacial recombination must retain sufficient reduction and oxidation potentials to drive the corresponding surface reactions. COFs offer substantial flexibility in this regard because their frontier-orbital energies can be regulated by the choice of building blocks, donor–acceptor motifs, conjugated linkages, heteroatoms, and functional groups. This molecular tunability enables both the energetic relationship with the coupled semiconductor and the redox capability of the retained carriers to be adjusted.

Experimentally, optical absorption spectroscopy is commonly combined with ultraviolet photoelectron spectroscopy (UPS), VB-XPS, and electrochemical measurements to establish the relative energy levels of the two components. In a COF/$BiVO_4$ S-scheme heterojunction, for example, the COF exhibits a more negative reduction level, whereas $BiVO_4$ provides a more positive oxidation level, an energetic configuration compatible with the retention of strongly reducing electrons on the COF and strongly oxidising holes on $BiVO_4$ (Figure 3a–c) [73]. Similar analyses of COF/CdS (Figure 3d–f) and COF/$ZnIn_2S_4$ (Figure 3g–l) heterojunctions have been used to assess whether the carriers retained by the proposed pathway possess sufficient energetic driving force for the target reduction and oxidation reactions [74,75].

However, for COF-based systems, conventional semiconductor analysis requires particular care. Depending on the extent of conjugation and carrier delocalisation, COFs may exhibit molecular-orbital, excitonic, and semiconductor-like characteristics simultaneously. Therefore, highest occupied molecular orbital (HOMO)/lowest unoccupied molecular orbital (LUMO) energies, optical transition energies, and electrochemically estimated band edges should not be treated as interchangeable quantities without justification. Likewise, Mott–Schottky analysis of highly porous or weakly conducting COFs can be influenced by frequency dispersion, surface states, interfacial capacitance, and departures from the assumptions of an ideal inorganic semiconductor. Therefore, electrochemical estimates should be cross-checked, whenever possible, against spectroscopic measurements and electronic-structure calculations.

Most importantly, energetic alignment establishes only whether a proposed pathway is plausible. Similar staggered configurations can support either a traditional type-II or an S-scheme interpretation, and the actual direction in which photogenerated carriers migrate cannot be inferred from the isolated energy levels alone. Therefore, band alignment should be regarded as a necessary energetic constraint rather than as direct evidence of S-scheme charge transfer.

Ground-state interfacial charge redistribution and IEFs

Next, energetic feasibility must be connected to the electronic structure that develops after interfacial contact. As described in Section 2, differences in the work functions and Fermi levels of the two components can induce electron redistribution until equilibrium is established, producing local charge accumulation and depletion, band bending, and an IEF. Therefore, evidence for this contact-induced reconstruction is required to establish the ground-state physical basis of a proposed S-scheme interface.

Work-function measurements and calculations provide an initial prediction of the direction of electron transfer. UPS, Kelvin probe force microscopy (KPFM) measurements, and calculated electrostatic-potential profiles can establish the relative Fermi-level positions of the isolated components, whereas measurements and calculations on the coupled heterointerface can test whether the predicted redistribution actually occurs. The $FeWO_4$/COF system provides a representative example. Calculated work functions of 5.73 and 6.13 eV for the COF and $FeWO_4$, respectively, predict electron transfer from the COF towards $FeWO_4$ upon contact (Figure 4a, b). Charge-density-difference calculations correspondingly show electron depletion on the COF and accumulation on $FeWO_4$ (Figure 4c), while dark-state XPS and KPFM measurements (Figure 4d–f) reveal electronic changes consistent with interfacial equilibration [76].

Nevertheless, COF-based interfaces introduce an additional interpretive challenge because charge redistribution may originate from more than global Fermi-level equilibration. **Coordination bonds, covalent bridges, donor–acceptor interactions, and local framework polarisation** can themselves redistribute electron density near the interface. Therefore, an XPS shift observed after heterojunction formation may contain contributions from both local bond-induced polarisation and broader interfacial equilibration. These effects should not automatically be treated as equivalent evidence for IEF formation. This distinction is particularly important for the coordination-mediated and covalently bridged interfaces discussed in Section 3, in which the chemical bond itself can substantially modify the local electronic structure.

Controlled interface modification can help separate these contributions. In nitrogen-vacancy-rich g-C_3N_4/Tp-Tta COF heterojunctions (Figure 4g, h), for example, the introduction of N vacancies shifts the electronic structure of g-C_3N_4 and increases its energetic offset relative to the COF, which is expected to favour a stronger interfacial electric field. The DFT-calculated work functions of Tp-Tta COF, pristine g-C_3N_4, and nitrogen-deficient g-C_3N_4 are 5.026, 4.658, and 4.425 eV, respectively. Therefore, the corresponding work-function difference relative to Tp-Tta COF increases from 0.368 to 0.601 eV upon nitrogen-vacancy introduction, indicating an enlarged Fermi-level offset between the two components. The N 1*s* XPS spectra further support changes in the local electronic environment of nitrogen species associated with vacancy introduction and interfacial coupling (Figure 4i). Such comparisons are mechanistically useful because they deliberately perturb the energetic asymmetry while retaining a related interface. However, the corresponding enhancement in CO_2 reduction activity cannot be used to quantify the field because vacancies may simultaneously affect adsorption, catalytic sites, carrier trapping, and reaction kinetics [48].

Therefore, the complementary roles and limitations of indi-

DOI: 10.68642/fuel.202600003

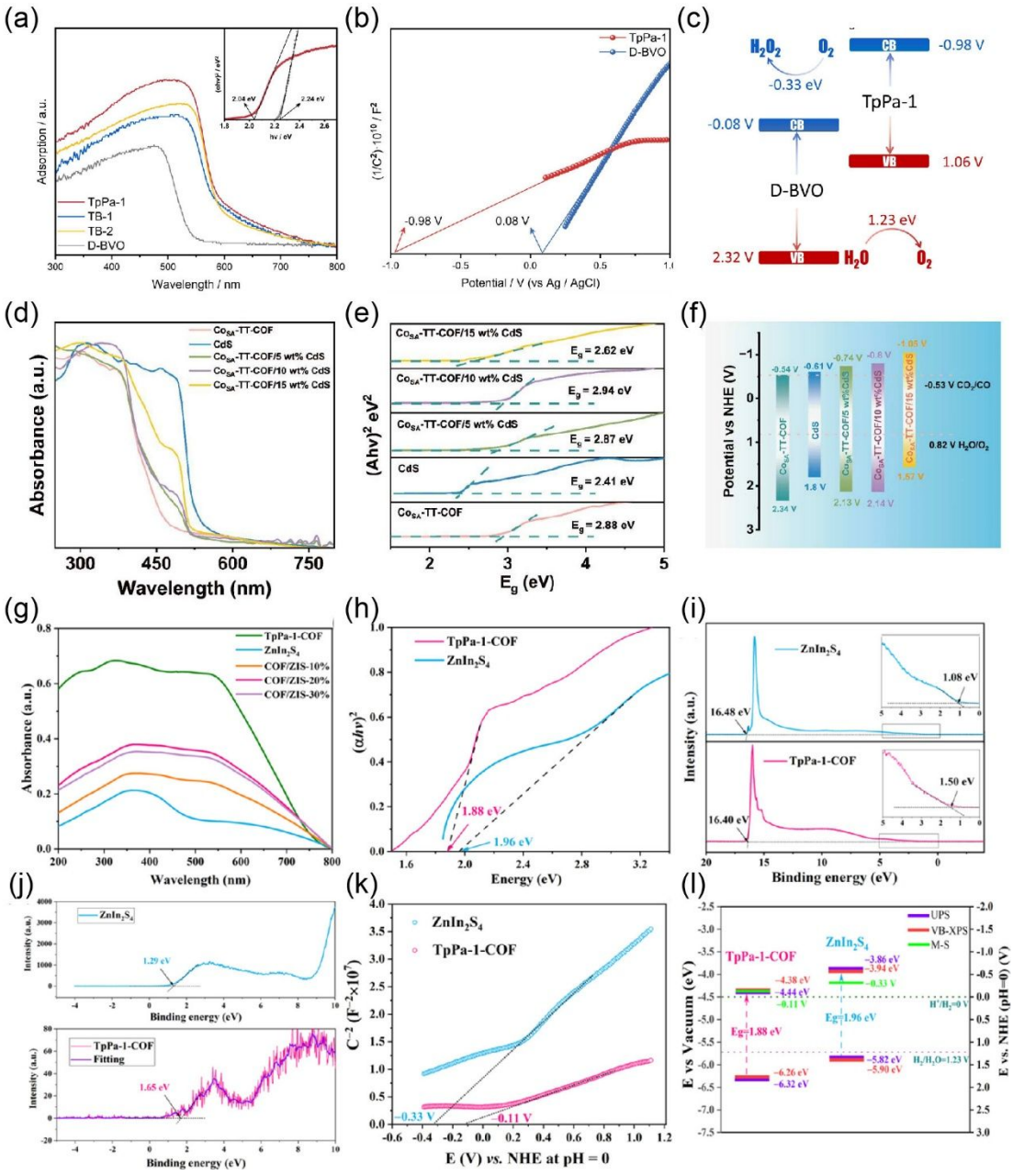


Fig. 3 Energy-level characterisation and band alignment of representative covalent organic framework (COF)-based heterojunctions. (a–c) Ultraviolet–visible (UV–vis) diffuse reflectance spectra with the corresponding Tauc plots in the inset, Mott–Schottky plots, and band alignment of the TpPa-1/$BiVO_4$ system, respectively. (d–f) UV–vis diffuse reflectance spectra, Tauc plots, and band-edge positions of CdS, CoSA-TT-COF, and CoSA-TT-COF/CdS composites with different CdS contents, respectively. (g) UV–vis diffuse reflectance spectra of TpPa-1-COF, $ZnIn_2S_4$, and their composites. (h) Tauc plots of TpPa-1-COF and $ZnIn_2S_4$. (i–k) Ultraviolet photoelectron spectroscopy (UPS) spectra, valence-band X-ray photoelectron spectroscopy (VB-XPS) spectra, and Mott–Schottky plots of TpPa-1-COF and $ZnIn_2S_4$, respectively. (l) Comparison of energy-level positions determined using UPS, VB-XPS, and Mott–Schottky analysis. (a–c) Reproduced from Ref. [73]. (d–f) Reproduced from Ref. [74]. (g–l) Reproduced from Ref. [75].

vidual techniques must be recognised. Work-function differences predict the expected direction of equilibration; charge-density-difference maps and Bader analysis describe redistribution within a specific structural model; dark-state XPS probes element-specific electronic responses; and KPFM measures local surface-potential variations. None of these techniques independently constitutes a direct measurement of a buried IEF. In porous COF heterostructures, the issue is further complicated when the relevant interface is located inside pores or beneath an outer COF layer, because the surface potential detected by KPFM may not faithfully represent the buried junction. Therefore, a reliable interpretation requires agreement among multiple measurements and consistency with the chemically realistic interfacial structure.

Photoinduced carrier distribution and dynamics

Ground-state interfacial reconstruction establishes the electronic landscape from which photoinduced transfer proceeds, but it does not determine where the photogenerated electrons and holes are ultimately retained. Therefore, evidence under illumination must address two complementary questions: which component hosts the surviving carriers with sufficient redox

DOI: 10.68642/fuel.202600003

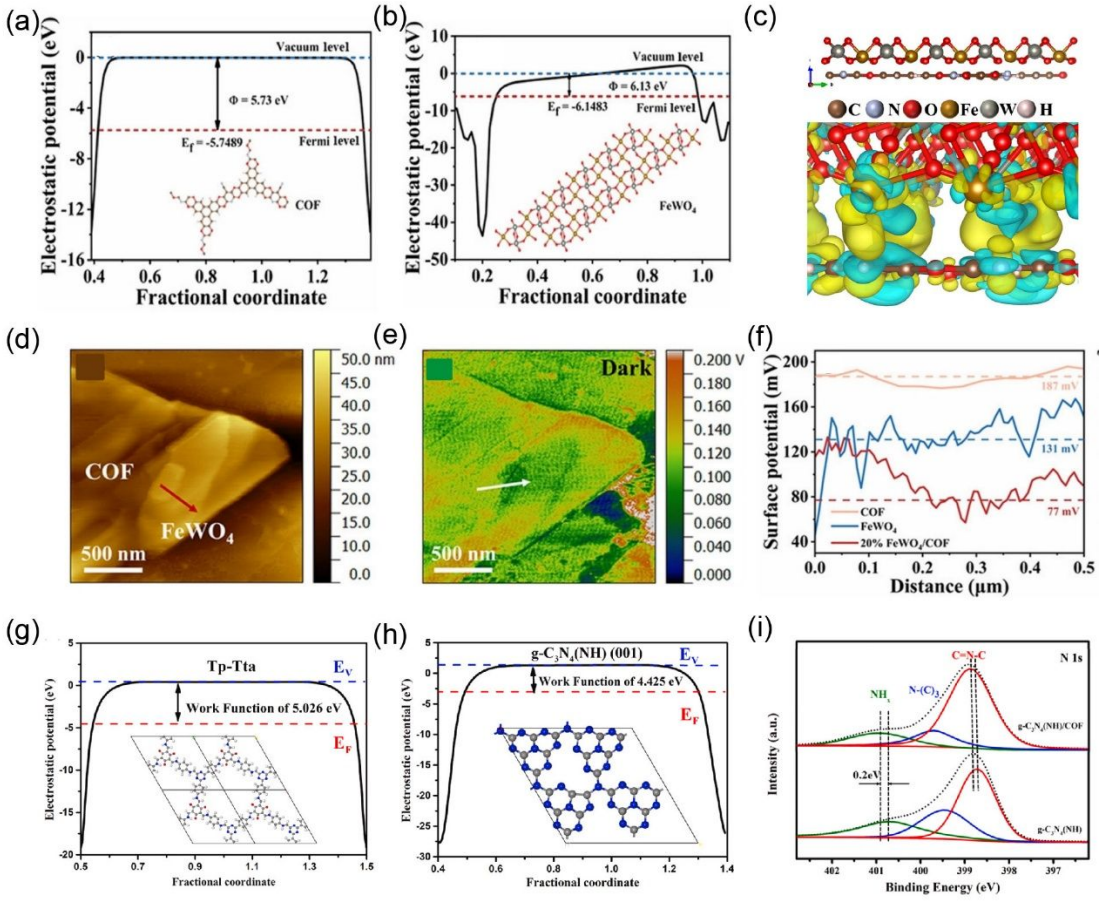


Fig. 4 Ground-state interfacial charge redistribution in representative covalent organic framework (COF)-based heterojunctions. (a, b) Calculated electrostatic potential profiles and work functions of COF and $FeWO_4$, respectively. (c) Structural model and calculated charge-density difference of the $FeWO_4$/COF interface. (d, e) Atomic force microscopy topography and corresponding dark-state Kelvin probe force microscopy surface-potential map of 20% $FeWO_4$/COF, respectively. (f) Surface-potential profiles of COF, $FeWO_4$, and 20% $FeWO_4$/COF. (g, h) Calculated electrostatic potential profiles and work functions of Tp-Tta COF and defective g-C_3N_4(NH), respectively. (i) High-resolution N 1*s* X-ray photoelectron spectra of g-C_3N_4(NH) and g-C_3N_4(NH)/COF. (a–f) Reproduced from Ref. [76]. (g–i) Reproduced from Ref. [48].

capability, and whether the observed excited-state dynamics are consistent with the proposed interfacial pathway.

Light-induced EPR and radical trapping provide functional information about the redox capability of the retained carriers. In the $FeWO_4$/COF heterojunction (Figure 5a), illumination produces a pronounced 5,5-dimethyl-1-pyrroline N-oxide (DMPO)–•O_2^- signal, whereas $FeWO_4$ alone yields no detectable signal. The commonly cited O_2/•O_2^- reduction potential is approximately −0.33 V vs. the normal hydrogen electrode (NHE), while the reported CB potentials of the COF and $FeWO_4$ are −0.79 and −0.32 V vs. NHE, respectively. Accordingly, electrons retained on the COF possess sufficient nominal reducing power for O_2 reduction, whereas electrons accumulated on $FeWO_4$ under a conventional type-II pathway would be marginally insufficient according to these values. Because •O_2^- formation requires sufficiently reducing electrons, this result supports the retention of strongly reducing electrons on the COF. Meanwhile, no discernible DMPO–•OH signals are observed for $FeWO_4$, the COF, or their heterojunction under illumination (Figure 5b). Such experiments can be highly discriminating when radical formation requires a redox potential clearly beyond that accessible through the competing traditional type-II pathway. Nevertheless, they remain functional probes of redox capability rather than direct tracers of electron migration, and the signal intensity can also be affected by reactant adsorption, pore accessibility, radical lifetime, and the local chemical environment of the COF [76].

Component-resolved XPS under illumination provides more direct information on carrier redistribution. In $FeWO_4$/COF (Figure 5c–f), COF-related C 1*s* and N 1*s* signals shift towards lower binding energies under illumination, whereas the Fe 2*p* and W 4*f* signals shift in the opposite direction, supporting photoinduced electron accumulation on the COF and electron depletion from $FeWO_4$. Importantly, this redistribution is opposite in direction to the dark-state electron transfer that occurs during interfacial equilibration. Complementary behaviour is observed in COF/ZnSe heterostructures, where dark-state equilibration transfers electrons from ZnSe towards the COF, whereas XPS under irradiation supports retention of photogenerated electrons on ZnSe and holes on the COF. Therefore, comparing component-specific signals in the same heterojunction under dark and illuminated conditions provides substantially stronger mechanistic discrimination than energy-level analysis alone [51,76].

Light-dependent KPFM and surface-photovoltage measurements provide complementary spatial information, but their interpretation is especially sensitive to COF morphology. Porous frameworks, encapsulated nanoparticles, core–shell

DOI: 10.68642/fuel.202600003

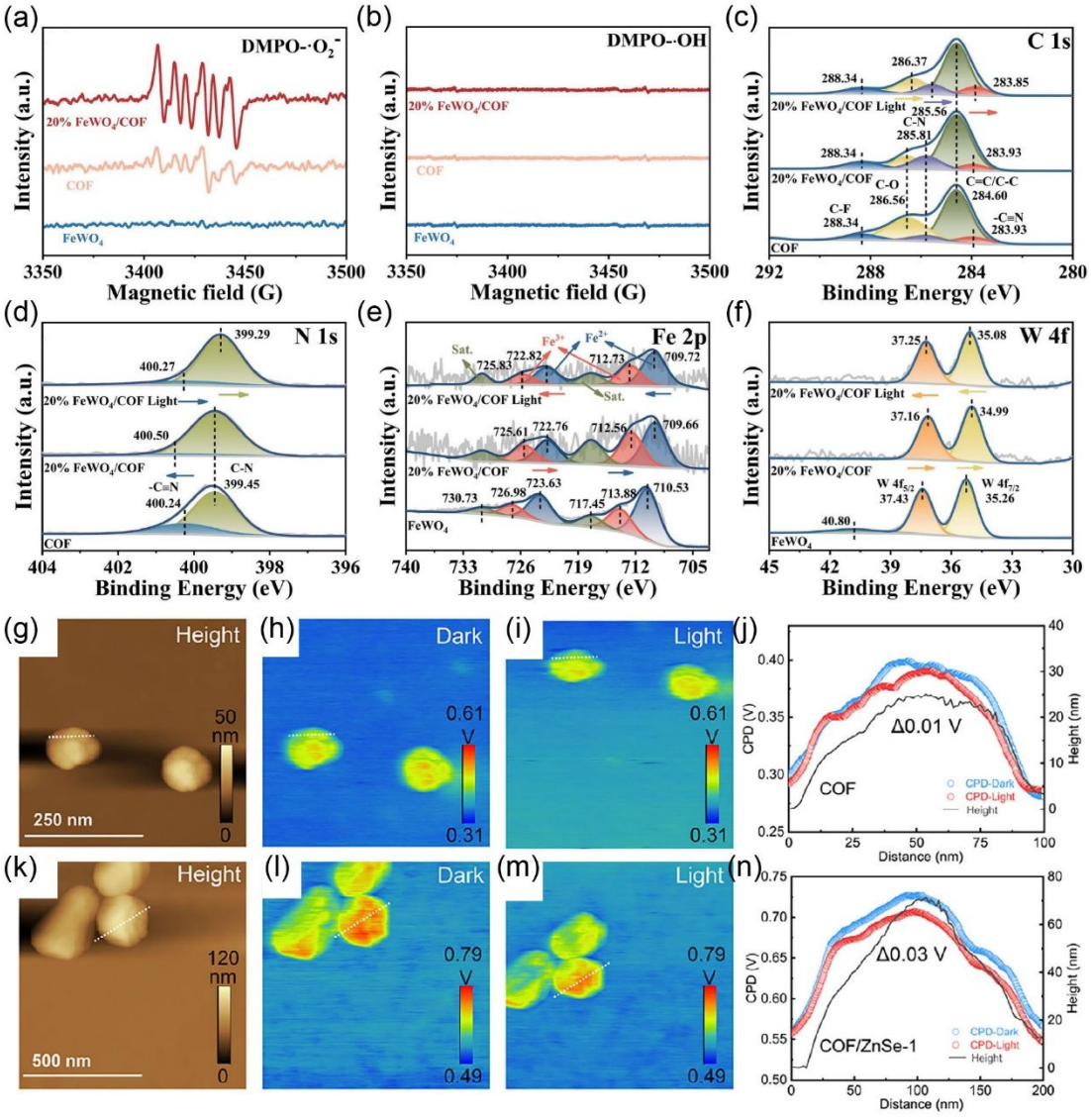


Fig. 5 Illumination-dependent identification of carrier location and redox capability in representative covalent organic framework (COF)-based step-scheme heterojunctions. (a, b) Light-induced electron paramagnetic resonance spectra of 5,5-dimethyl-1-pyrroline N-oxide (DMPO)–•O_2^- and DMPO–•OH adducts for COF, $FeWO_4$, and 20% $FeWO_4$/COF. (c–f) C 1*s*, N 1*s*, Fe 2*p*, and W 4*f* X-ray photoelectron spectra of the isolated components and 20% $FeWO_4$/COF under dark and illuminated conditions. (g–j) Atomic force microscopy (AFM) height image, dark- and light-state contact-potential-difference maps, and corresponding line profiles of the isolated COF. (k–n) Corresponding AFM and Kelvin probe force microscopy results for COF/ZnSe-1. (a–f) Reproduced from Ref. [76]. (g–n) Reproduced from Ref. [51].

architectures, and confined quantum dots can place the electronically active interface beneath the externally accessible surface. For example, in COF/ZnSe (Figure 5g–n), an increased light-induced surface-potential response is consistent with enhanced charge separation, but an overall potential change at the outer COF surface cannot independently identify the carrier distribution at a buried COF/ZnSe interface. Therefore, spatially resolved potential measurements are most informative when chemically distinct regions of the interface can be resolved and correlated with component-specific spectroscopic evidence.

Time-resolved spectroscopy adds a kinetic dimension, but COFs again require special caution. In particular, fs-TAS can resolve excited-state formation, intraframework relaxation, exciton dissociation, trapping, and interfacial transfer on overlapping timescales. In donor–acceptor COFs, changes in decay kinetics may arise from intrinsic charge-transfer states or framework relaxation even in the absence of a heterointerface. Therefore, an additional kinetic component appearing after heterojunction formation should not automatically be assigned to interfacial charge transfer [77,78].

In TPA-COF/$CsPbBr_3$ quantum-dot heterostructures, an additional decay component that emerges after coupling is attributed to an interface-associated pathway (Figure 6a–d). Its mechanistic significance becomes convincing only when it is interpreted together with independent electronic-structure and carrier-location evidence [79]. A similar principle applies to COF/ZnSe, where heterostructure formation accelerates the decay of COF-related transient features (Figure 6e–k). XPS under irradiation independently locates the retained electrons on ZnSe, allowing the faster depletion of the monitored COF state to be associated with selective interfacial transfer [51]. Therefore, the value of fs-TAS lies not simply in observing a faster or slower decay but in identifying which electronic state is depleted, which state is populated, and whether the resulting

DOI: 10.68642/fuel.202600003

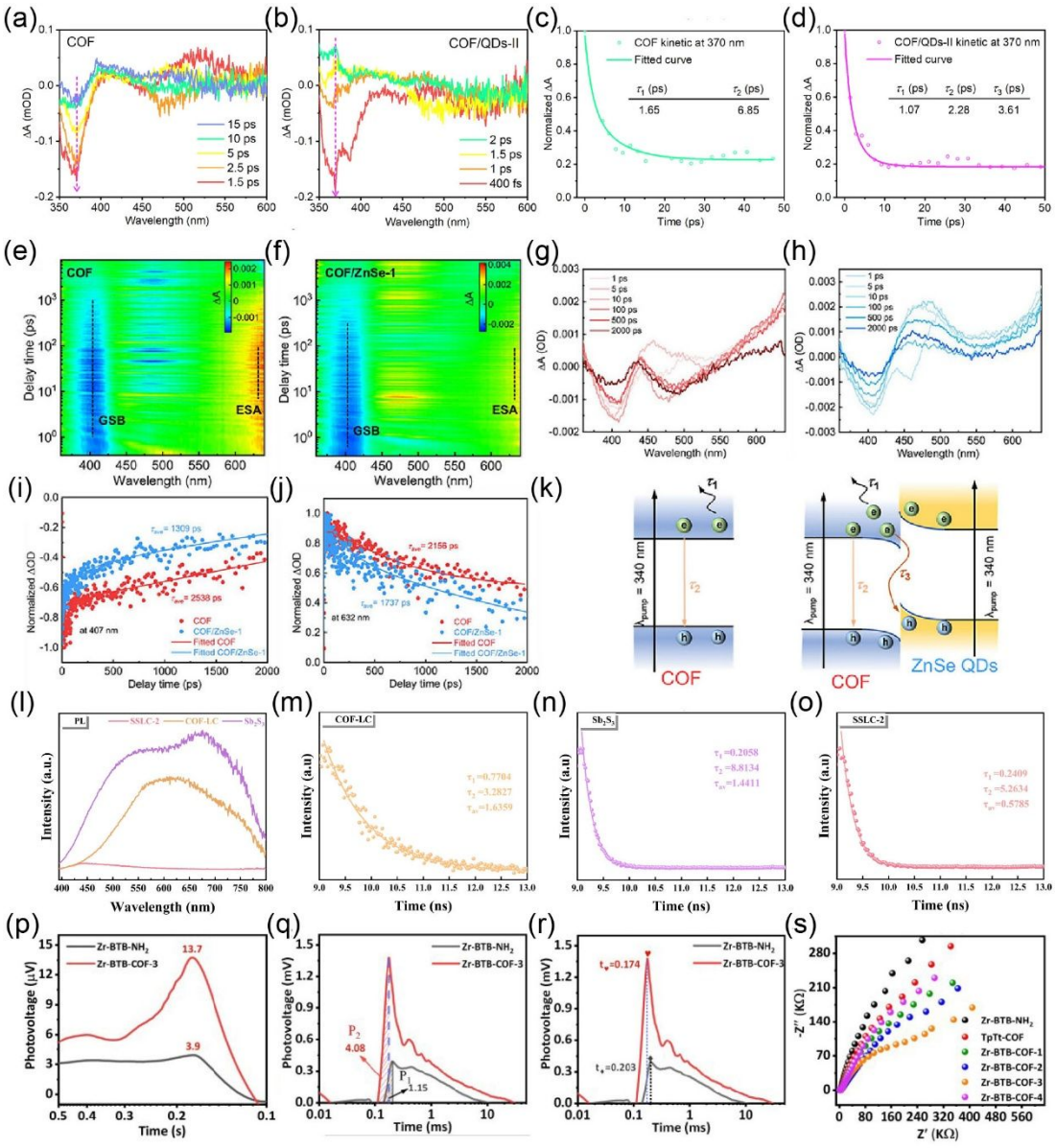


Fig. 6 Multiscale characterisation of interfacial charge transfer, excited-state relaxation, and surface-charge extraction in covalent organic framework (COF)-based step-scheme heterojunctions. (a, b) Transient-absorption spectra of TPA-COF and TPA-COF/$CsPbBr_3$ quantum dots recorded at selected delay times. (c, d) Corresponding normalised decay kinetics monitored at 370 nm. (e, f) Two-dimensional transient-absorption maps of the isolated COF and COF/ZnSe-1. (g, h) Transient-absorption spectra recorded at selected delay times. (i, j) Normalised decay kinetics monitored at 407 and 632 nm, respectively. (k) Proposed excited-state relaxation and interfacial-transfer pathways in the isolated COF and COF/ZnSe heterostructure. (l) Steady-state photoluminescence (PL) spectra of COF-LC, Sb_2S_3, and SSLC-2. (m–o) Corresponding time-resolved PL decay profiles. (p) Transient surface-photovoltage responses of Zr-BTB-NH_2 and Zr-BTB-COF-3. (q, r) Charge-extraction responses and maximum extraction times. (s) Electrochemical impedance spectroscopy Nyquist plots of Zr-BTB-NH_2, TpTt-COF, and Zr-BTB-COF composites. (a–d) Reproduced from Ref. [79]. (e–k) Reproduced from Ref. [51]. (l–o) Reproduced from Ref. [69]. (p–s) Reproduced from Ref. [70].

kinetics agree with the independently established carrier distribution.

Measurements beyond the femtosecond regime are required to determine whether early-time transfer generates useful, longer-lived, and surface-accessible charges (Figure 6l–o). Time-resolved photoluminescence (PL) spectroscopy can reveal additional depopulation channels of emissive states, but changes in lifetime may also reflect aggregation, interlayer coupling, defect trapping, or nonradiative relaxation intrinsic to the COF. In the Zr-BTB-COF system, transient surface-photovoltage and charge-extraction measurements and electrochemical impedance spectroscopy provide complementary information on charge separation, extraction, and interfacial transport, respectively (Figure 6p–s). None of these techniques alone identifies the microscopic transfer pathway. Therefore, a robust mechanistic picture requires temporal continuity from early-time state depletion to longer-lived charge accumulation, together with independent determination of the component on which the surviving carriers reside [69,70,80].

Evidence hierarchy and common pitfalls in S-scheme assignment

A reliable S-scheme assignment in a COF-based heterojunction requires a coherent chain of evidence spanning energetic feasibil-

DOI: 10.68642/fuel.202600003

ity, ground-state interfacial reconstruction, and photoinduced carrier behaviour. These three levels address different mechanistic questions and cannot substitute for one another. Energetic analysis constrains which carrier-transfer pathways are thermodynamically possible; dark-state measurements establish whether interfacial contact produces the expected electronic reconstruction; and illumination-dependent and time-resolved measurements determine whether the photogenerated carriers are redistributed and evolve consistently with the proposed S-scheme pathway (Figure 7). Therefore, the strength of an assignment depends less on the number of techniques employed than on whether independent observations converge on the same mechanistic picture. Accordingly, no individual measurement is sufficient to establish the complete S-scheme pathway [17,27,30].

For COF-based heterojunctions, this requirement is particularly important because several intrinsic features of COFs can mimic or complicate signatures commonly attributed to S-scheme formation. For example, interfacial XPS shifts may reflect not only Fermi-level equilibration but also coordination-induced polarisation, covalent bond formation, framework charging, or local chemical reconstruction. Likewise, charge-density-difference calculations describe a specific structural model, whereas real COF interfaces may contain multiple bonding motifs, defects, orientations, and degrees of disorder. KPFM adds spatial information but probes the surface contact potential rather than directly probing a buried electric field; in porous, encapsulated, or confined heterostructures, the measured outer-surface potential may not represent the electrostatics of the active internal junction. Therefore, ground-state charge redistribution should be established through mutually consistent structural, spectroscopic, electrostatic, and theoretical evidence rather than inferred from a single binding-energy or surface-potential shift.

Photoinduced measurements present a second source of possible overinterpretation. In COFs, intraframework donor–acceptor transfer, exciton migration, interlayer transport, defect trapping, and nonradiative relaxation can occur on timescales that overlap with those of interfacial carrier transfer. Consequently, the appearance of an additional transient component, PL quenching, or a shorter excited-state lifetime after heterojunction formation does not by itself identify an S-scheme pathway. Conversely, a longer-lived state is not necessarily catalytically beneficial if the corresponding carriers are trapped or inaccessible to reactants. Time-resolved signals are mechanistically meaningful only when the monitored species are reliably assigned and their kinetic evolution is consistent with independently established carrier locations under illumination [77–79].

Functional redox probes should be interpreted with the same caution. EPR-detected radicals, selective photodeposition, and probe reactions can demonstrate that sufficiently reducing or oxidising carriers are present, but they do not directly trace the microscopic migration pathway. Their diagnostic value is greatest when the redox threshold of the detected process can discriminate the proposed S-scheme pathway from competing charge-transfer models. Similarly, enhanced photocurrent, lower electrochemical impedance, stronger surface photovoltage, and improved photocatalytic activity indicate changes in charge transport or utilisation but cannot by themselves distinguish S-scheme transfer from traditional type-II behaviour.

This distinction is especially important for COF-based photocatalysts because interface construction often alters the reaction environment while modifying charge transfer. Changes in porosity, local polarity, CO_2 enrichment, proton accessibility, active-site exposure, and intermediate stabilisation can all enhance catalytic performance independently of the carrier-migration pathway. Therefore, improved CO_2 conversion or

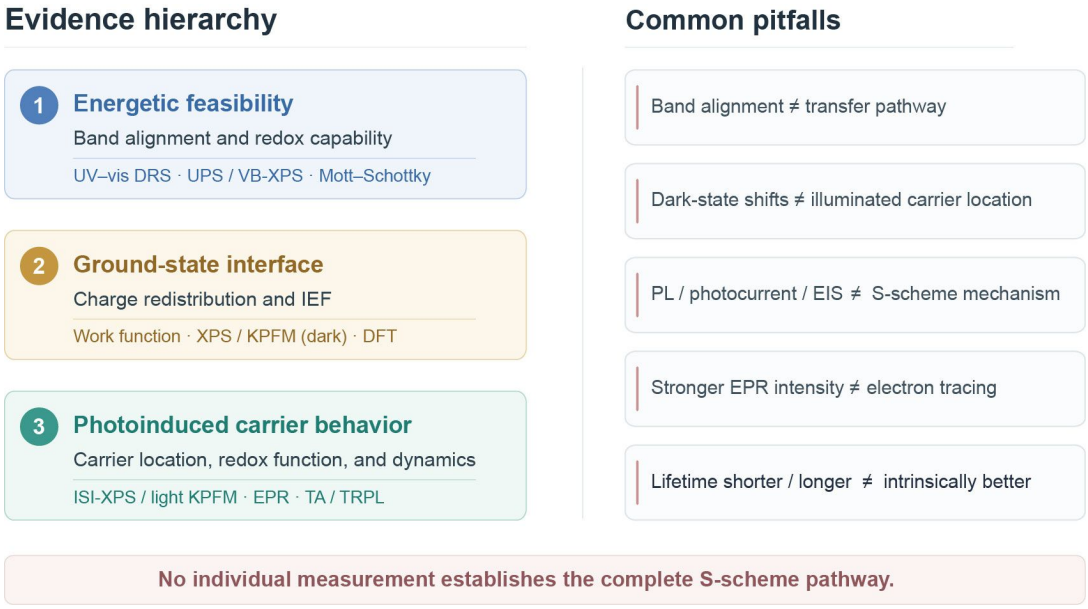


Fig. 7 Evidence hierarchy and covalent organic framework-specific pitfalls in establishing step-scheme charge transfer. Conceptual schematic based on Refs [17,27,30]. DFT, density functional theory; EIS, electrochemical impedance spectroscopy; EPR, electron paramagnetic resonance; ISI-XPS, *in situ* irradiated X-ray photoelectron spectroscopy; KPFM, Kelvin probe force microscopy; PL, photoluminescence; TA, transient absorption; TRPL, time-resolved photoluminescence; UPS, ultraviolet photoelectron spectroscopy; UV–vis DRS, ultraviolet–visible diffuse reflectance spectroscopy; VB-XPS, valence-band X-ray photoelectron spectroscopy; XPS, X-ray photoelectron spectroscopy.

DOI: 10.68642/fuel.202600003

altered product selectivity should not be used as direct evidence for an S-scheme mechanism unless the contribution of these parallel structural and chemical effects is separately considered.

Taken together, a robust S-scheme assignment should satisfy a causal sequence rather than a checklist of characterisation methods. The proposed energetic configuration must first be internally consistent with the required redox chemistry; interfacial contact must then produce a physically plausible electronic reconstruction; illumination must generate a carrier distribution compatible with the proposed RP/OP roles; and the corresponding carrier dynamics must support, rather than contradict, that distribution. For COF-based heterojunctions, an additional requirement is to distinguish genuinely interfacial phenomena from responses originating within the COF itself or from changes in the porous reaction microenvironment. Only when these independent constraints converge, and plausible alternatives such as traditional type-II transfer are disfavoured, can an S-scheme pathway be assigned with confidence.

From Interfacial Charge Migration to CO_2 Conversion Chemistry

Establishing an S-scheme charge-transfer pathway identifies where photogenerated electrons and holes are preferentially retained, but it does not by itself explain catalytic activity or product selectivity. The retained electrons must still reach adsorbed CO_2-derived species, participate in the required electron–proton transfer steps, and outcompete alternative sinks such as proton reduction. Therefore, charge separation and productive charge utilisation are distinct but coupled processes: the former determines the availability and redox capability of photogenerated carriers, whereas the latter is governed by the chemical environment in which those carriers are consumed.

APTES, (3-aminopropyl)triethoxysilane; bpy, 2,2′-bipyridine; COF, covalent organic framework; HER, hydrogen evolution reaction; MeCN, acetonitrile; PMBA, p-methoxybenzyl alcohol; QDs, quantum dots; S-scheme, step-scheme; TEOA, triethanolamine; UV, ultraviolet.

This distinction is particularly important for COF-based S-scheme photocatalysts. In addition to light harvesting and charge transport, COFs provide porous reaction spaces, chemically programmable adsorption sites, coordination environments, and tunable local polarity. Interfacial construction can further modify these properties by redistributing electron density and placing charge-accumulation regions close to catalytic sites. Consequently, the catalytic outcome depends not simply on how many charges are separated but on how electron delivery is coupled with CO_2 enrichment, site-specific adsorption, proton availability, intermediate stabilisation, and product desorption. The following sections examine this progression from initial CO_2 activation to two-electron reduction and, ultimately, to the branching of multielectron pathways. Representative COF-based S-scheme photocatalysts are summarised in Table 5, together with their main products, catalytic performance, reaction conditions, and proposed interfacial functions.

CO_2 adsorption and initial molecular activation

Strongly reducing electrons retained through an S-scheme pathway can contribute to CO_2 conversion only if they are delivered to chemically accessible CO_2 molecules. Therefore, for COF-

Table 5 Representative COF-based S-scheme photocatalysts for CO_2 reduction, including catalytic performance, reaction conditions, and proposed interfacial roles.

Photocatalyst	Product(s)	Activity ($\mu mol\ g^{-1}\ h^{-1}$)/ selectivity	Key conditions	Proposed interfacial role
g-C_3N_4(NH)/Tp-Tta COF [48]	CO	562.5; 90.4%	>400 nm; MeCN/H_2O/TEOA; Co/bpy	Defect-regulated transfer and CO_2 adsorption
$FeWO_4$/COF [76]	CO	55.9; 100%	Simulated sunlight; MeCN/H_2O; no sacrificial agent	Site-specific CO_2 adsorption and reduction
Zr-BTB-COF [70]	CO	71.9; >99%	300 W Xe; H_2O/PMBA	Covalent coupling and paired alcohol oxidation
APTES–Cu_2O/COF [68]	CO, CH_4	CO: 5.63; ≈89%	300 W Xe, full spectrum; MeCN/TEOA	Facilitated *COOH formation; HER competition
COF-5@$CsPbBr_3$ [81]	CO, CH_4	CO: 52.70; 82.4%	≥420 nm; MeCN/H_2O/TEOA	Electron delivery to $CsPbBr_3$
TPT-COF/ZnO QDs [60]	CH_4, CO	CH_4: 3.92; ≈80%	UV–visible light; CO_2/H_2O; no sacrificial agent	Zn–N coupling and CO_2 activation
NM(S)/F@T [82]	CH_4	154.3; 87.4%	CO_2/H_2O	Facet-dependent hydrogen supply and hydrogenation
CdS/$BiVO_4$@T-COF [83]	CO + H_2	Total: 453.6; CO: 40.5%	300 W Xe, 420–780 nm; CO_2/H_2O/MeCN	CO_2 enrichment and spatial reaction separation
IS@COF-Ni [84]	C_2H_4	49.2; 86.3%	Visible light; H_2O vapour; no sacrificial agent	*CO retention and C–C coupling

DOI: 10.68642/fuel.202600003

based photocatalysts, three related but distinct functions should be distinguished: enrichment of CO_2 within the porous framework, preferential adsorption at specific chemical sites, and electron-induced activation of the adsorbed molecule. High CO_2 uptake can increase the local reactant concentration, but it does not necessarily identify the sites involved in catalysis or indicate that the adsorbed molecules are productively activated. Therefore, the relevant design objective is not maximum adsorption alone but the spatial and electronic coupling of accessible CO_2-binding sites with the retained photogenerated electrons [85–87].

The dual S-scheme CdS/$BiVO_4$@T-COF system illustrates the first level of this relationship. Thickening the porous T-COF shell progressively increases CO_2 uptake, demonstrating that the COF can act as a tunable reservoir for local reactant enrichment (Figure 8a). CO_2 temperature-programmed desorption further reveals stronger CO_2 interactions with T-COF than with CdS (Figure 8b), and theoretical calculations indicate more favourable CO2 adsorption and lower free-energy requirements for subsequent *COOH formation and CO release on the COF component (Figure 8c). These results connect reactant enrichment with a surface environment that can support subsequent reduction, but they also illustrate why adsorption capacity alone is an insufficient descriptor of catalytic utilisation [83].

Site-specific calculations provide a more chemically resolved picture. In the $FeWO_4$/COF S-scheme heterojunction, CO_2 adsorption at cyano-N, pyridinic-N, and dioxin-O sites gives calculated adsorption energies of −0.75, −0.51, and −0.53 eV, respectively, identifying the cyano-containing region as the strongest modelled binding site (Figure 8d). The corresponding free-energy profiles further show that the choice of local adsorption site affects not only initial CO2 binding but also the subse-

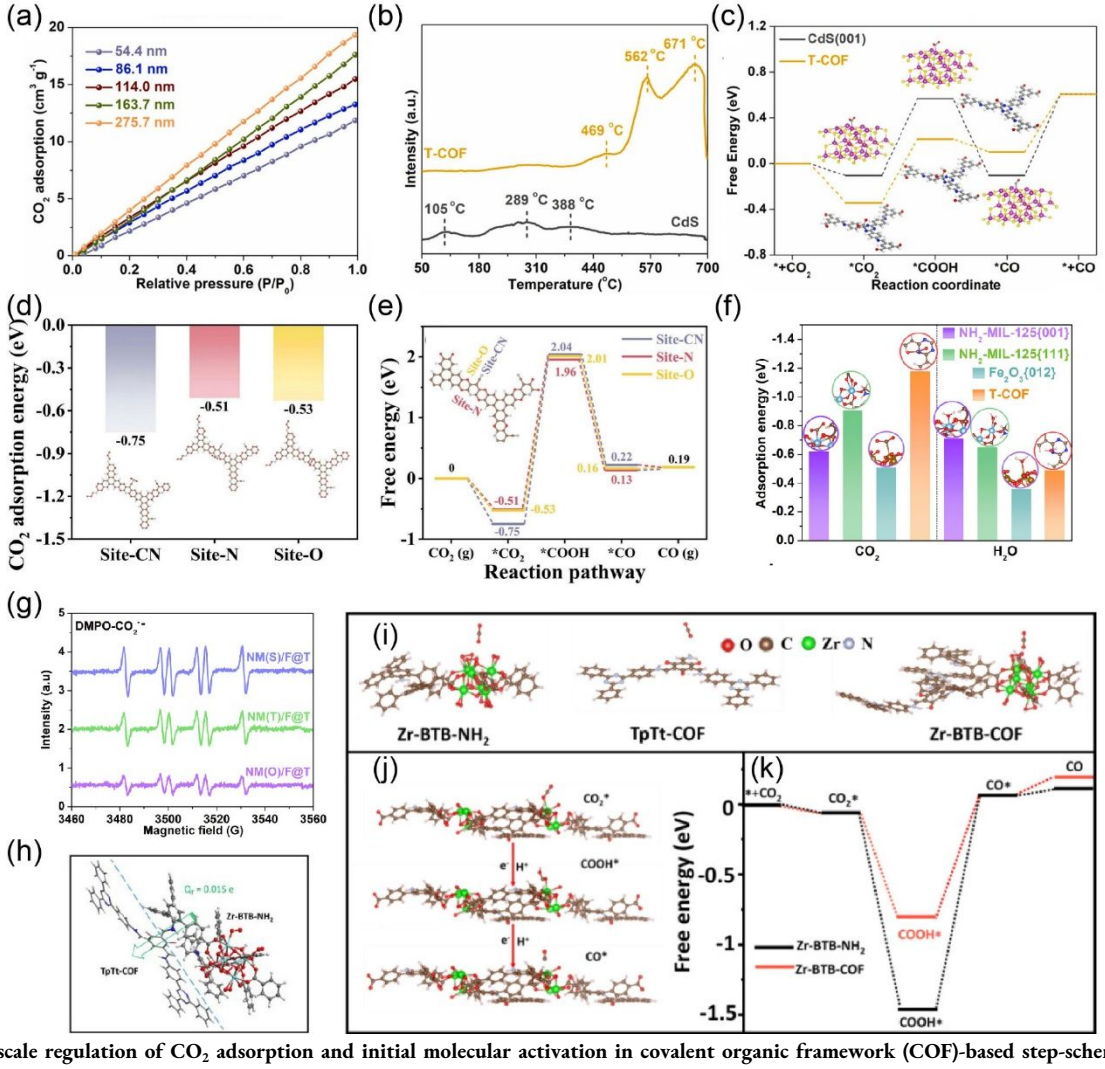


Fig. 8 Multiscale regulation of CO_2 adsorption and initial molecular activation in covalent organic framework (COF)-based step-scheme photocatalysts. (a) CO_2 adsorption isotherms of CdS/$BiVO_4$@T-COF composites with different T-COF shell thicknesses. (b) CO_2 temperature-programmed desorption profiles of T-COF and CdS. (c) Calculated Gibbs free-energy profiles for CO_2-to-CO conversion on CdS(001) and T-COF. (d) Calculated CO_2 adsorption energies at the cyano-N (Site-CN), pyridinic-N (Site-N), and dioxin-O (Site-O) sites of the COF. (e) Corresponding Gibbs free-energy profiles for CO_2 reduction at the three COF sites. (f) Calculated adsorption energies of CO_2 and H_2O on NH_2-MIL-125 (001), NH_2-MIL-125 (111), Fe_2O_3 (012), and T-COF, showing component-dependent adsorption preferences. (g) EPR spectra of DMPO–$CO_2^{\bullet-}$ adducts over facet-engineered NH_2-MIL-125/Fe_2O_3/T-COF composites under illumination. (h) DFT-derived interfacial charge redistribution and transferred charge between TpTt-COF and Zr-BTB-NH_2 in the covalently coupled Zr-BTB-COF heterostructure. (i) Optimised CO_2 adsorption configurations on Zr-BTB-NH_2, TpTt-COF, and Zr-BTB-COF. (j) Optimised configurations of *CO_2, *COOH, and *CO intermediates on Zr-BTB-COF. (k) Gibbs free-energy profiles for CO_2-to-CO conversion over Zr-BTB-NH_2 and Zr-BTB-COF. (a–c) Reproduced from Ref. [83]. (d, e) Reproduced from Ref. [76]. (f, g) Reproduced from Ref. [82]. (h–k) Reproduced from Ref. [70].

DOI: 10.68642/fuel.202600003

quent energetics of *COOH and *CO formation (Figure 8e). Thus, adsorption strength and reaction thermodynamics are linked through the local chemical structure of the COF rather than through the total CO_2 uptake of the material [76].

COF-containing multicomponent heterojunctions can also partition different reactants among spatially distinct regions. In the NH_2-MIL-125/Fe_2O_3/T-COF dual S-scheme system, calculated CO_2 adsorption is substantially more favourable on T-COF than on the exposed NH_2-MIL-125 and Fe_2O_3 surfaces, whereas H_2O preferentially interacts with NH_2-MIL-125 (Figure 8f). This spatial differentiation provides a possible way to regulate separately CO_2 activation and proton/hydrogen supply. The stronger DMPO–$CO_2^{\bullet-}$ response of the optimised composite under illumination (Figure 8g) is consistent with more effective one-electron activation of CO_2, although the radical signal itself reflects both carrier availability and the local adsorption environment [82].

Importantly, heterointerface formation can also modify the adsorption site itself. In the β-ketoenamine-bridged Zr-BTB-COF heterostructure, calculated interfacial charge redistribution between TpTt-COF and Zr-BTB-NH_2 changes the local electronic environment of the coupled region (Figure 8h). Correspondingly, the calculated CO_2 adsorption energy is more favourable at the heterostructure than on either isolated component (Figure 8i), while the optimised *CO_2, *COOH, and *CO configurations and the associated free-energy profiles indicate facilitated progression along the CO_2-to-CO pathway (Figure 8j, k). In this case, the heterointerface functions not only as a conduit for carrier migration but also as an electronically reconstructed reaction region [70].

These examples show that the contribution of a COF to initial CO_2 conversion cannot be reduced to a high surface area or a large adsorption capacity. Productive activation requires a sequence of coupled functions: local enrichment increases molecular availability, chemically defined sites determine adsorption geometry and binding strength, and interfacial electronic coupling determines whether those adsorbates can access sufficiently reducing electrons. Distinguishing these functions is essential because a large population of adsorbed CO_2 does not necessarily translate into a large population of catalytically productive CO_2.

Two-electron CO_2 reduction: CO formation and selectivity

Both CO and formate/formic acid can arise from two-electron CO_2 reduction. However, among the COF-based S-scheme systems surveyed in this Review, CO formation is much more commonly reported; therefore, it is used here as the representative two-electron pathway. Its formation is usually described by the sequence CO_2 → *COOH → *CO → CO. Retaining strongly reducing electrons through an S-scheme pathway can provide the energetic basis for these elementary steps, but electron availability alone does not determine the rate or selectivity of CO formation. The catalytic site must facilitate *COOH formation and subsequent conversion while suppressing competing proton reduction, and the resulting *CO must be released before further hydrogenation occurs. Therefore, CO selectivity emerges from the balance among electron delivery, *COOH formation, *H adsorption, and *CO binding [40,88].

The COF-5@$CsPbBr_3$ heterojunction illustrates the link between S-scheme charge retention and CO formation. In the proposed charge-transfer pathway, strongly reducing electrons remain on $CsPbBr_3$ (Figure 9a). *In situ* diffuse reflectance infrared Fourier transform spectroscopy (DRIFTS) under CO_2 reveals light-dependent changes in bands assigned to carbon-containing surface species, including *COOH and *CO, thereby linking the proposed electron distribution to the evolution of reaction intermediates (Figure 9b, c). The *in situ* grown heterostructure produces substantially more CO than its physically mixed counterpart (Figure 9d, e), consistent with more effective utilisation of photogenerated charges for CO_2 reduction after intimate interfacial coupling. However, both CO and CH_4 formation increase after coupling. Therefore, the results support enhanced CO production and a changed product distribution, but they do not by themselves demonstrate that the interface selectively suppresses further hydrogenation of *CO [81].

A clearer example of competition between CO_2 reduction and hydrogen evolution is provided by the covalently coupled (3-aminopropyl)triethoxysilane (APTES)–Cu_2O/COF heterojunction. The proposed S-scheme pathway retains strongly reducing electrons on Cu_2O, while interfacial covalent coupling produces a substantially higher CO yield than that obtained with the corresponding physically mixed or more weakly coupled systems (Figure 9f). *In situ* DRIFTS detects *COOH- and *CO-related species during irradiation (Figure 9g). More importantly, calculations show that the free-energy requirement for *COOH formation decreases to 0.85 eV on the coupled system, compared with 2.55 and 2.67 eV on Cu_2O and the COF, respectively (Figure 9h). In the same model, the formation of adsorbed *H is less favourable on the composite (Figure 9i). Together with the absence of detectable H_2 under the reported reaction conditions, these results support the preferential utilisation of reducing equivalents by the CO_2-to-CO pathway rather than by proton reduction [68].

The two systems illustrate why CO selectivity should not be inferred directly from improved charge separation. S-scheme charge migration determines where strongly reducing electrons remain available, whereas the local catalytic environment determines how these electrons are partitioned among *COOH formation, hydrogen evolution, and further conversion of *CO. Therefore, efficient and selective CO production requires simultaneous control of carrier supply and surface thermodynamics: CO_2 activation must be favoured over *H formation, while *CO binding must remain sufficiently moderate to permit desorption. When *CO is retained and supplied with additional electrons and hydrogen equivalents, the reaction instead proceeds along the multielectron pathways discussed below [89,90].

Multielectron reduction and competing reaction pathways

Multielectron CO_2 reduction introduces an additional requirement beyond retaining strongly reducing electrons: the carrier supply must be temporally and spatially matched to proton transfer and intermediate stabilisation over a sequence of

DOI: 10.68642/fuel.202600003

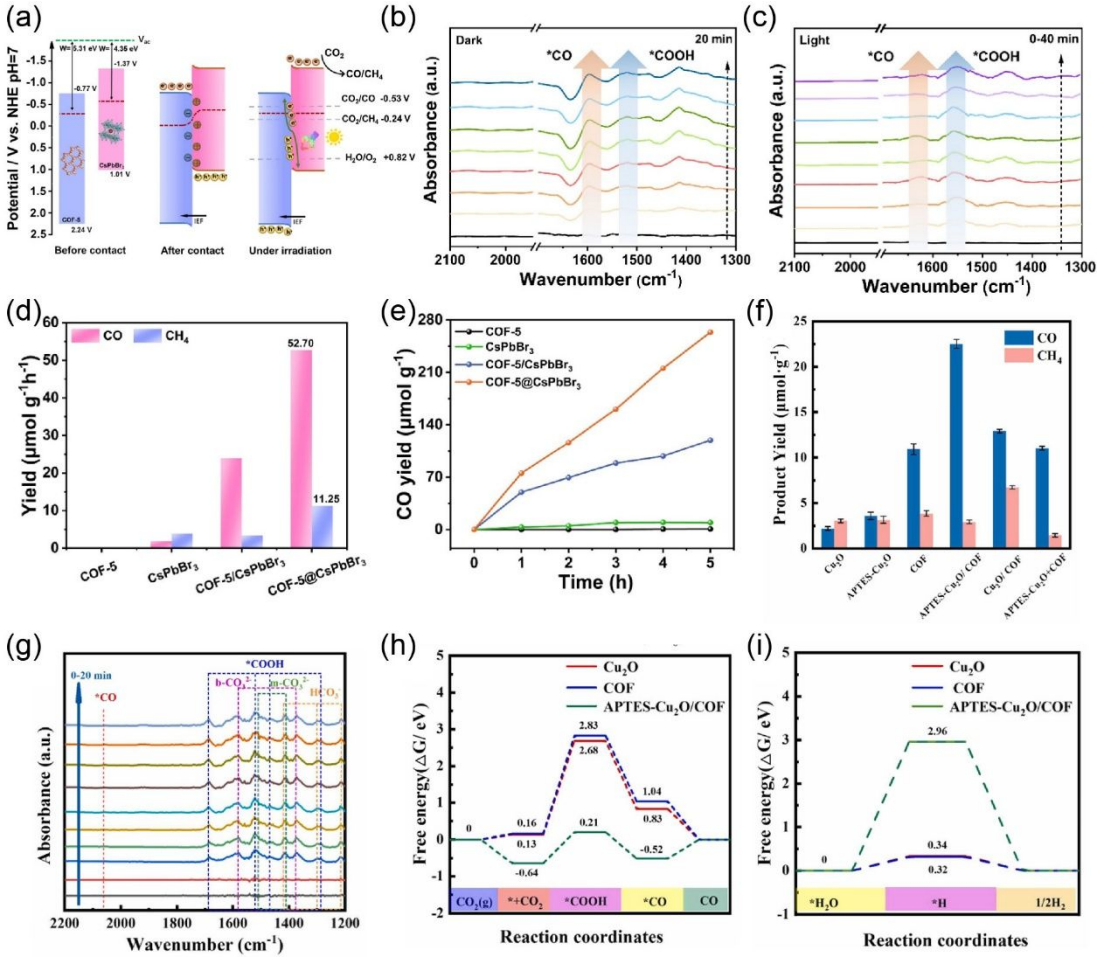


Fig. 9 Linking step-scheme charge migration to surface intermediates and CO_2-to-CO conversion in covalent organic framework (COF)-based heterojunctions. (a) Proposed charge-transfer mechanism of COF-5@$CsPbBr_3$. (b, c) *In situ* diffuse reflectance infrared Fourier transform spectroscopy (DRIFTS) spectra of CO_2 interacting with COF-5@$CsPbBr_3$ in the dark and under visible-light irradiation, respectively. (d) CO and CH_4 production rates and (e) time-dependent CO yields over COF-5, $CsPbBr_3$, physically mixed COF-5/$CsPbBr_3$, and *in situ* grown COF-5@$CsPbBr_3$ under visible-light irradiation ($\lambda \geq 420$ nm). (f) CO and CH_4 yields over Cu_2O, (3-aminopropyl)triethoxysilane (APTES)–Cu_2O, COF, and their coupled or physically mixed composites after 4 h of irradiation. (g) *In situ* DRIFTS spectra of APTES–Cu_2O/COF during CO_2 photoreduction. (h, i) DFT-calculated Gibbs free-energy profiles for the CO_2-to-CO pathway and hydrogen evolution, respectively, on the isolated components and coupled interface. (a–e) Reproduced from Ref. [81]. (f–i) Reproduced from Ref. [68].

elementary steps. For CO-derived pathways, adsorbed *CO is a major branching point. Desorption terminates reduction at CO and successive hydrogenation can direct the reaction towards CH_4, whereas the retention of multiple neighbouring CO-derived species can enable C–C coupling and the subsequent formation of C_2 products. An S-scheme heterojunction can determine where and how persistently reducing electrons are supplied, but the chemical environment in which *CO is formed and retained selects the eventual reaction branch [91–93].

The facet-controlled NH_2-MIL-125/Fe_2O_3/T-COF dual S-scheme system illustrates how electron supply can be coupled with hydrogen availability to regulate the depth of reduction. Changing the exposed facets of the metal–organic framework component alters the performance of an otherwise related heterojunction architecture. The {001}-rich NM(S)/F@T sample gives the highest CH_4 production and selectivity, whereas shifting the exposed facets towards those of NM(O)/F@T decreases CH_4 formation, increases CO production, and produces a smaller amount of C_2H_4 (Figure 10a–c). This trend suggests that product branching is associated not only with electron availability at the T-COF reduction region but also with facet-dependent water activation and hydrogen supply [82].

The accompanying mechanistic evidence supports this interpretation while defining its limits. Calculations on T-COF show that the conversion of *CO towards *CHO is energetically preferred over CO desorption in the modelled pathway (Figure 10d). The NM(S)/F@T sample also displays the strongest DMPO–H response under Ar and the largest decrease in this signal after the introduction of CO_2 (Figure 10e, f), consistent with increased participation of reactive hydrogen species during CO_2 conversion. Taken together, the product distribution, reaction energetics, and EPR responses support a picture in which sustained electron delivery to the COF region is matched with hydrogen availability, enabling successive *CO hydrogenation towards CH_4. Importantly, the calculation establishes the intrinsic energetic preference of the modelled T-COF surface; it does not by itself demonstrate that the formation of the S-scheme heterojunction lowers the elementary barrier for *CO hydrogenation.

DOI: 10.68642/fuel.202600003

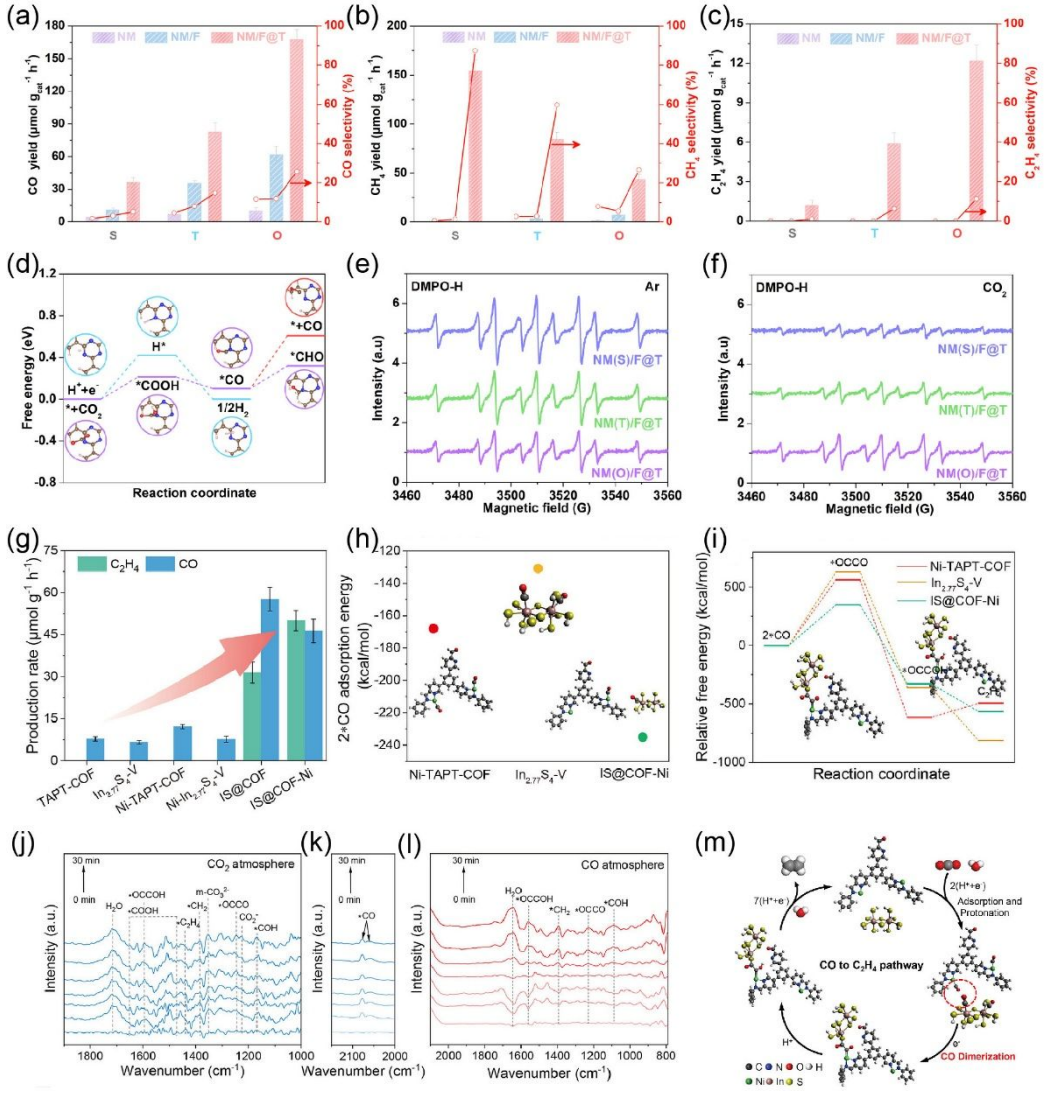


Fig. 10 Interfacial regulation of multielectron CO_2 reduction in covalent organic framework (COF)-based step-scheme photocatalysts. (a–c) CO, CH_4, and C_2H_4 yields and selectivities over facet-controlled NH_2-MIL-125/Fe_2O_3/T-COF composites. NM denotes NH_2-MIL-125. S, T, and O indicate sheet-like, truncated-octahedral, and octahedral morphologies, respectively, with reported exposed {111} facet fractions of 43%, 78%, and 100%. F denotes Fe_2O_3, and @T indicates coating with a T-COF shell. (d) Calculated free-energy pathways for CO_2 reduction and H_2 evolution on T-COF. (e, f) DMPO–H EPR spectra collected under (e) Ar and (f) CO_2. (g) CO and C_2H_4 production rates of the indium sulfide/COF-based samples. IS@COF denotes a heterostructure comprising nonstoichiometric indium sulfide (IS) and an imine–pyridine COF; IS@COF-Ni additionally incorporates isolated Ni sites at the interfacial edges. (h) Calculated adsorption energies of two *CO species and (i) free-energy profiles involving *OCCO formation. (j, k) *In situ* diffuse reflectance infrared Fourier transform (DRIFTS) spectra collected under CO_2, including the *CO spectral region, and (l) spectra collected under CO. (m) Proposed pathway for the conversion of CO-derived intermediates to C_2H_4. (a–f) Reproduced from Ref. [82]. (g–m) Reproduced from Ref. [84].

A different outcome emerges when the interface favours the accumulation and proximity of CO-derived intermediates rather than successive hydrogenation. In the IS@COF-Ni system, the isolated components predominantly produce CO, whereas the formation of the IS@COF heterojunction enables C_2H_4 production. Introducing isolated Ni sites at the interfacial edges further increases the C_2H_4 formation rate to 49.2 μmol g^{-1} h^{-1} while decreasing CO production relative to IS@COF (Figure 10g). This comparison suggests complementary roles for heterojunction formation and interfacial Ni sites: the former sustains the supply of reducing equivalents and the formation of CO-derived species, whereas the latter provides sites that favour their retention and spatial proximity [84].

The calculated and spectroscopic results further support this branch. The assembled interface shows more favourable retention of two *CO species and a more favourable pathway involving the coupling-associated *OCCO configuration (Figure 10h, i). Under CO_2, *in situ* infrared spectra contain bands assigned to *CO and C_2-related intermediates (Figure 10j, k), while complementary measurements under CO probe the subsequent chemistry of CO-derived species (Figure 10l). Together, these observations are consistent with a sequence in which neighbouring *CO species accumulate in the interfacial region, undergo C–C coupling, and are subsequently converted towards C_2H_4 (Figure 10m). In this case, stronger charge separation alone would not explain the product shift; the decisive factor is the coupling of sustained electron supply with an interfacial site arrangement that can stabilise adjacent carbon-containing intermediates.

The contrast between these systems reveals the chemically

DOI: 10.68642/fuel.202600003

relevant role of S-scheme charge migration in multielectron CO_2 conversion. The heterojunction determines the location, redox energy, and continuity of the electron supply, but it does not uniquely prescribe the product. Where electron delivery is matched with efficient hydrogen transfer and the sequential stabilisation of hydrogenated intermediates, *CO can proceed towards CH_4. Where the interface instead promotes the accumulation and proximity of multiple *CO species, the same reducing equivalents can be directed towards C–C coupling. Therefore, product selectivity emerges from matching charge delivery to a specific intermediate network rather than from maximising charge separation in isolation [94–97].

This coupling highlights a distinctive opportunity for COF-based S-scheme photocatalysts: charge redistribution, intermediate binding, and reactant/proton transport can, in principle, be integrated within the same molecularly programmable architecture. Therefore, the next design challenge is not simply to retain more energetic carriers but to synchronise their delivery with reactant enrichment, proton transfer, and intermediate evolution at structurally defined catalytic sites. Achieving such coordination will be essential for moving from efficient charge separation to predictable control of multielectron and higher-value CO_2 conversion [98,99].

Challenges and Perspectives

COF-based S-scheme heterojunctions provide an attractive platform for integrating interfacial charge regulation with molecularly programmable reaction environments. However, the next stage of development requires moving beyond the empirical assumption that improved charge separation necessarily leads to better CO_2 conversion. As discussed throughout this Review, favourable energy-level alignment does not establish the actual charge-transfer pathway, efficient carrier separation does not guarantee productive charge utilisation, and the retention of strongly reducing electrons does not by itself determine whether CO_2 reduction terminates at CO or proceeds towards deeply reduced or multicarbon products. Therefore, future progress depends on establishing causal relationships among interfacial structure, charge migration, catalytic-site chemistry, and reaction branching. The central challenge is no longer simply how to construct an S-scheme heterojunction but how to design an interface that delivers the appropriate carriers to the appropriate reaction sites at the rate required by a targeted chemical pathway.

Towards structurally defined and operando-validated S-scheme interfaces

The electronic behaviour of a COF-based heterojunction is governed by its local interfacial structure rather than by its nominal composition alone. Noncovalent contacts, coordination bonds, covalent bridges, defects, different stacking arrangements, and weakly coupled domains may coexist within the same material. The exposed facets or surface terminations of the coupled component can further alter orbital overlap, local electrostatics, and charge redistribution. Consequently, an idealised structural model or evidence of morphological contact cannot by itself reveal which interface is responsible for the observed charge-transfer behaviour.

Therefore, a major priority is to develop structurally controlled heterointerfaces in which bonding configuration, orientation, interfacial distance, or defect population can be varied independently while other parameters are kept as constant as possible. With such model systems, changes in charge redistribution and transfer kinetics could be linked to specific structural variables rather than to uncontrolled differences in particle size, porosity, crystallinity, or composition. For COFs, this will require close attention to the molecular identity of interfacial binding sites, framework stacking, linkage chemistry, and the distribution of chemically distinct coordination environments. Likewise, calculations should move beyond idealised interfaces whenever possible and be constrained by experimentally supported structures.

The relevant interface may also differ between the as-prepared material and the working photocatalyst. CO_2 adsorption, protonation, coordination of reaction intermediates, light-induced charging, and local structural reconstruction can modify interfacial dipoles and electronic coupling under reaction conditions. Therefore, *ex situ* characterisation provides only a partial description of the catalytically active interface. Future studies should increasingly combine operando structural and electronic probes with illumination-dependent potential mapping and time-resolved spectroscopy to determine whether the interfacial configuration proposed for the pristine material remains valid during photocatalysis. The key mechanistic question should shift from whether a composite is compatible with an S-scheme description to which chemically defined interface sustains the observed charge-transfer pathway under operating conditions.

Linking charge migration with catalytic chemistry

A second challenge is to determine which separated carrier populations are catalytically competent. Rather than treating lifetime extension or rapid interfacial transfer as independent performance targets, future studies should establish whether spectroscopically identified carrier populations participate directly in active-site reduction, intermediate conversion, and product formation.

The principal difficulty is the temporal gap between initial photoexcitation and catalytic turnover. Ultrafast spectroscopy can resolve exciton formation, intraframework relaxation, and early interfacial transfer, whereas CO_2 adsorption, proton transfer, intermediate transformation, and product formation generally occur over much longer timescales. Establishing causality across these regimes requires measurements that connect carrier dynamics with the evolution of chemically defined states rather than examine the two processes independently. Therefore, time-resolved spectroscopy should be combined with operando vibrational spectroscopy, X-ray methods, isotope experiments, kinetic measurements, and reaction-state calculations capable of tracking the formation and consumption of intermediates such as *COOH, *OCHO, *CO, and *CHO.

Controlled perturbation provides an additional route to establishing this connection. Changes in photon flux, excitation mode, CO_2 pressure, water activity, proton-donor concentra-

tion, or reactant composition can alter the rates of carrier generation and consumption differently. If changes in carrier populations, catalytic-state formation, intermediate coverage, and product formation respond consistently to such perturbations, a stronger causal connection can be established between photophysics and reaction chemistry. Conversely, an increase in carrier lifetime without a corresponding change in intermediate evolution or catalytic turnover would indicate that the accumulated charges are not kinetically relevant to the rate-determining chemistry.

Ultimately, productive photocatalysis requires matching electron and proton fluxes to the kinetics of individual elementary steps. Increasing electron delivery will be of little benefit if proton transfer, intermediate conversion, or product desorption remains limiting; the excess carriers may instead recombine or be consumed by hydrogen evolution. Likewise, accelerating interfacial transfer without controlling where the transferred charges accumulate may increase the population of electronically separated but catalytically inaccessible carriers. Therefore, IEFs, rapid charge transfer, and long carrier lifetimes should be regarded as tools for supplying chemically usable charges rather than as independent design objectives.

Towards selective and higher-value CO_2 conversion

Future COF-based S-scheme photocatalysts should increasingly be designed from the desired reaction pathway backwards rather than from charge separation forwards. Selective CO formation, deep reduction to CH_4 or CH_3OH, and C_{2+} production impose fundamentally different requirements on intermediate binding, proton delivery, active-site arrangement, and carrier supply. CO remains an important target product, and deeper reduction should not automatically be regarded as superior. Efficient CO production requires favourable *COOH formation and conversion together with sufficiently facile *CO desorption, whereas CH_4 or CH_3OH formation requires sustained electron/proton delivery and controlled progression through successive hydrogenation and C–O bond transformation steps. C_{2+} formation imposes even more stringent requirements, including sufficient surface coverage of carbon-containing intermediates, neighbouring active sites, and geometries that permit productive C–C coupling.

The molecular programmability of COFs offers an unusual opportunity to coordinate these requirements within a single architecture. Pore size, polarity, wettability, proton-relay groups, coordination sites, and spatial confinement could be adjusted to regulate CO_2 enrichment, proton accessibility, intermediate residence time, and communication between adjacent catalytic sites. However, these variables cannot be optimised independently. Increasing local proton availability may accelerate hydrogenation but simultaneously promote H_2 evolution; strengthening *CO adsorption may favour downstream conversion but suppress CO desorption and site regeneration; stronger confinement may increase the residence time of intermediates but impede mass transport. Therefore, future design should focus on reaction-specific combinations of charge supply, intermediate binding, and microenvironment rather than on maximising any single descriptor.

The same principle applies to higher-value transformations beyond conventional C_1 reduction. COF-based heterostructures may provide spatially organised environments for C–C or C–heteroatom bond formation, including C–N coupling, as well as for combining CO_2 reduction with selective oxidation reactions. Such transformations require substantially stronger mechanistic validation than the mere simultaneous detection of products from two half-reactions. Isotope tracing, carbon and electron balances, intermediate identification, control reactions, and the exclusion of parallel pathways are required to demonstrate genuine catalytic coupling. Spatially differentiated COF architectures may be particularly useful in this context because reduction sites, oxidation sites, proton-transfer networks, and molecular-transport pathways can, in principle, be positioned within distinct but electronically connected regions.

Therefore, a product-oriented design strategy begins with the decisive intermediate and elementary step, defines the required electronic and chemical environment, and only then selects the interfacial architecture needed to provide that environment. This approach differs fundamentally from conventional optimisation, which begins by maximising charge separation and then evaluates whichever reaction pathway emerges. Instead, the target product defines the required carrier flux, proton availability, intermediate binding, and active-site arrangement before the interface is designed. COFs should not be viewed merely as porous supports or tunable energy-level components, and the assignment of an S-scheme pathway should not substitute for the identification of the catalytic mechanism. When structurally defined interfaces, carrier dynamics, proton and reactant transport, intermediate evolution, and product formation can be connected within a single experimentally testable framework, COF-based S-scheme photocatalysts can progress from empirically assembled heterojunctions towards rationally designed platforms for selective and higher-value CO_2 conversion.

Acknowledgements

This work was supported by the National Natural Science Foundation of China (22378371, 22361142704, 22238009, U24A2071, and W2512051), the Natural Science Foundation of Hubei Province of China (2025AFD020), and the Fundamental Research Funds for the Central Universities, China University of Geosciences (Wuhan) (No. CUG22061).

Conflict of Interest

The authors declare no conflict of interest.

Data Availability Statement

No new data were generated in this study. All information discussed in this Review is derived from the cited publications and their Supporting Information.

This is an open access article under the terms of the Creative Commons Attribution 4.0 International License (CC BY 4.0, https://creativecommons.org/licenses/by/4.0/).
© The Author(s) 2027.

Reference and Notes

1. L. Wang, B. Zhu, J. Zhang, J. B. Ghasemi, M. Mousavi, J. Yu. S-scheme heterojunction photocatalysts for CO_2 reduction. *Matter* **2022**, 5, 4187–4211. DOI: 10.1016/j.matt.2022.09.009

2. S. Fang, M. Rahaman, J. Bharti, E. Reisner, M. Robert, G. A. Ozin, Y. H. Hu. Photocatalytic CO_2 reduction. *Nat. Rev. Methods Primers* **2023**, 3, 61. DOI: 10.1038/s43586-023-00243-w
3. F. Kolahdouzan, N. Goodarzi, M. Setayeshmehr, D. S. Mousavi, A. Z. Moshfegh. 1D-based nanostructures in photocatalytic CO_2 reduction. *Chin. J. Catal.* **2025**, 70, 230–259. DOI: 10.1016/S1872-2067(24)60214-7
4. J. Cheng, B. Cheng, J. Xu, J. Yu, S. Cao. Organic–inorganic S-scheme heterojunction photocatalysts: Design, synthesis, applications, and challenges. *eScience* **2025**, 5, 100354. DOI: 10.1016/j.esci.2024.100354
5. X. Li, J. Yu, M. Jaroniec, X. Chen. Cocatalysts for Selective Photoreduction of CO_2 into Solar Fuels. *Chem. Rev.* **2019**, 119, 3962–4179. DOI: 10.1021/acs.chemrev.8b00400
6. Y. Amao. Photo/Biohybrid Catalytic System for Application in Semiartificial Photosynthesis of CO_2 to Chemicals. *Chem. Rev.* **2026**, 126, 1635–1685. DOI: 10.1021/acs.chemrev.5c00754
7. Y. Wang, E. Chen, J. Tang. Insight on Reaction Pathways of Photocatalytic CO_2 Conversion. *ACS Catal.* **2022**, 12, 7300–7316. DOI: 10.1021/acscatal.2c01012
8. T. Kong, Y. Jiang, Y. Xiong. Photocatalytic CO_2 conversion: What can we learn from conventional CO_x hydrogenation? Chem. *Soc. Rev.* **2020**, 49, 6579–6591. DOI: 10.1039/C9CS00920E
9. H. -K. Wu, Y. -H. Li, M. -Y. Qi, Q. Lin, Y. -J. Xu. Enhanced photocatalytic CO_2 reduction with suppressing H_2 evolution via Pt cocatalyst and surface SiO_2 coating. *Appl. Catal. B Environ. Energy* **2020**, 278, 119267
10. J. Low, J. Yu, M. Jaroniec, S. Wageh, A. A. Al-Ghamdi. Heterojunction Photocatalysts. *Adv. Mater.* **2017**, 29, 1601694. DOI: 10.1002/adma.201601694
11. Q. Xu, L. Zhang, B. Cheng, J. Fan, J. Yu. S-Scheme Heterojunction Photocatalyst. *Chem* **2020**, 6, 1543–1559. DOI: 10.1016/j.chempr.2020.06.010
12. M. Sayed, K. Qi, X. Wu, L. Zhang, H. García, J. Yu. Cu-based S-scheme photocatalysts. *Chem. Soc. Rev.* **2025**, 54, 4874–4921
13. X. Wu, G. Chen, J. Wang, J. Li, G. Wang. Review on S-Scheme Heterojunctions for Photocatalytic Hydrogen Evolution. *Acta Phys. Chim. Sin.* **2023**, 39, 2212016.
14. Z. -B. Fang, T. -T. Liu, J. Liu, S. Jin, X. -P. Wu, X. -Q. Gong, K. Wang, Q. Yin, T. -F. Liu, R. Cao, H. -C. Zhou. Boosting Interfacial Charge-Transfer Kinetics for Efficient Overall CO_2 Photoreduction via Rational Design of Coordination Spheres on Metal–Organic Frameworks. *J. Am. Chem. Soc.* **2020**, 142, 12515–12523
15. Q. Xu, S. Wageh, A. A. Al-Ghamdi, X. Li. Design principle of S-scheme heterojunction photocatalyst. *J. Mater. Sci. Technol.* **2022**, 124, 171–173. DOI: 10.1016/j.jmst.2022.02.016
16. L. Yang, Z. Wu, H. Hou, W. Chen, Y. Li. Recent advances in COF-based S-scheme photocatalyst. *J. Mater. Sci. Technol.* **2026**, 275, 271–285. DOI: 10.1016/j.jmst.2026.04.006
17. Y. Mo, X. Wen, Z. Ke, C. Huang, R. Shen, S. Wang, X. Li, J. Luo, X. Li. Interfacial engineering in COF-based S-scheme heterojunctions for enhanced photocatalysis. *Chin. Chem. Lett.* **2026**, 37, 113086. DOI: 10.1016/j.cclet.2026.113086
18. L. Zhao, K. Xu, C. Bie. 2D COF photocatalyst with highly stabilized tautomeric transition and singlet oxygen generation. *Acta Phys. Chim. Sin.* **2026**, 42, 100216. DOI: 10.1016/j.actphy.2025.100216
19. T. Li, N. Tsubaki, Z. Jin. S-scheme heterojunction in photocatalytic hydrogen production. *J. Mater. Sci. Technol.* **2024**, 169, 82–104. DOI: 10.1016/j.jmst.2023.04.049
20. X. Wu, C. Cheng. Chiral COF-based S-scheme heterojunction for spin-polarized photocatalytic hydrogen evolution. *Acta Phys. Chim. Sin.* **2026**, 42, 100303. DOI: 10.1016/j.actphy.2026.100303
21. F. Xie, C. Yuan, H. Tan, A. Z. Moshfegh, B. Zhu, J. Yu. d-Band Center Regulated O_2 Adsorption on Transition Metal Single Atoms Loaded COF: A DFT Study. *Acta Phys. Chim. Sin.* **2024**, 40, 2407013. DOI: 10.3866/PKU.WHXB202407013
22. F. Xie, C. Bie, J. Sun, Z. Zhang, B. Zhu. A DFT study on Pt single atom loaded COF for efficient photocatalytic CO_2 reduction. *J. Mater. Sci. Technol.* **2024**, 170, 87–94. DOI: 10.1016/j.jmst.2023.06.028
23. Y. Yang, J. Liu, M. Gu, B. Cheng, L. Wang, J. Yu. Bifunctional TiO_2/COF S-scheme photocatalyst with enhanced H_2O_2 production and furoic acid synthesis mechanism. *Appl. Catal. B Environ. Energy* **2023**, 333, 122780. DOI: 10.1016/j.apcatb.2023.122780
24. H. Zhang, J. Liu, Y. Zhang, B. Cheng, B. Zhu, L. Wang. BiOBr/COF S-scheme photocatalyst for H_2O_2 production via concerted two-electron pathway. *J. Mater. Sci. Technol.* **2023**, 166, 241–249. DOI: 10.1016/j.jmst.2023.05.030
25. X. Wang, H. Zhang, X. Zheng, J. Cui, M. Yu, H. Liu, Y. Zhao. Dimensional Isomerism in COFs Enabled by Spirobifluorene Substitution for Enhanced Photocatalytic CO_2 Reduction. *Angew. Chem. Int. Ed.* **2026**, 65, e1182476. DOI: 10.1002/anie.1182476
26. S. Wei, R. Hou, Q. Zhu, I. Shakir, Z. Fang, X. Duan, Y. Xu. Hybrid materials based on covalent organic frameworks for photocatalysis. *InfoMat* **2025**, 7, e12646. DOI: 10.1002/inf2.12646
27. X. Wu, M. Sayed, G. Wang, W. Yu, B. Zhu. COF-Based S-Scheme Heterojunction Photocatalyst. *Adv. Mater.* **2026**, 38, e11322. DOI: 10.1002/adma.202511322
28. H. Li, W. Wang, K. Xu, B. Cheng, J. Xu, S. Cao. Solar-driven H_2O_2 production by S-scheme heterojunction photocatalyst. *Chin. J. Catal.* **2025**, 72, 24–47. DOI: 10.1016/S1872-2067(24)60257-3
29. B. Zhu, C. Jiang, J. Xu, Z. Zhang, J. Fu, J. Yu. Quantum dots in S-scheme photocatalysts. *Mater. Today* **2025**, 82, 251–273. DOI: 10.1016/j.mattod.2024.11.012
30. L. Zhang, J. Zhang, J. Yu, H. García. Charge-transfer dynamics in S-scheme photocatalyst. *Nat. Rev. Chem.* **2025**, 9, 328–342
31. W. Wang, B. Cheng, G. Luo, J. Yu, S. Cao. S-scheme heterojunction photocatalysts based on 2D materials. *Mater. Today* **2024**, 81, 137–158. DOI: 10.1016/j.mattod.2024.10.006
32. K. Sayama, K. Mukasa, R. Abe, Y. Abe, H. Arakawa. Stoichiometric water splitting into H_2 and O_2 using a mixture of two different photocatalysts and an IO_3^-/I^- shuttle redox mediator under visible light irradiation. *Chem. Commun.* **2001**, 37, 2416–2417.
33. A. J. Bard. Photoelectrochemistry and heterogeneous photo-catalysis at semiconductors. *J. Photochem.* **1979**, 10, 59–75. DOI: 10.1016/0047-2670(79)80037-4
34. K. Sayama, K. Mukasa, R. Abe, Y. Abe, H. Arakawa. A new photocatalytic water splitting system under visible light irradiation mimicking a Z-scheme mechanism in photosynthesis. *J. Photochem. Photobiol. A Chem.* **2002**, 148, 71–77. DOI: 10.1016/S1010-6030(02)00070-9
35. H. Tada, T. Mitsui, T. Kiyonaga, T. Akita, K. Tanaka. All-solid-state Z-scheme in CdS–Au–TiO_2 three-component nanojunction system. *Nat. Mater.* **2006**, 5, 782–786. DOI: 10.1038/nmat1734
36. J. Yu, S. Wang, J. Low, W. Xiao. Enhanced photocatalytic performance of direct Z-scheme g-C_3N_4–TiO_2 photocatalysts for the decomposition of formaldehyde in air. *Phys. Chem. Chem. Phys.* **2013**, 15, 16883–16890. DOI: 10.1039/c3cp53131g
37. J. Fu, Q. Xu, J. Low, C. Jiang, J. Yu. Ultrathin 2D/2D WO_3/g-C_3N_4 step-scheme H_2-production photocatalyst. *Appl. Catal. B Environ. Energy* **2019**, 243, 556–565. DOI: 10.1016/j.apcatb.2018.11.011
38. M. Sayed, L. Zhang, H. García, H. Yu, J. Yu. S-Scheme Shapes Heterojunction Photocatalysis. *Acc. Chem. Res.* **2026**, 59, 1138–1153.
39. L. Qin, D. Sun, D. Ma, Z. Wang, Y. Liu, Q. Li, F. Song, K. Wu, L. Gan, T. Zhou, J. Zhang. Decoupling Interlayer Interactions Boosts Charge Separation in Covalent Organic Frameworks for High-Efficiency Photocatalytic CO_2 Reduction. *Adv. Mater.* **2025**, 37, 2504205. DOI: 10.1002/adma.202504205
40. Q. Niu, Q. Chen, G. Huang, L. Li, Y. He, J. Bi. Build-in electric field in $CuWO_4$/covalent organic frameworks S-scheme photocatalysts steer boosting charge transfer for photocatalytic CO_2 reduction. *J. Colloid Interface Sci.* **2023**, 643, 102–114. DOI: 10.1016/j.jcis.2023.04.013
41. H. Zhao, L. Wang, G. Liu, Y. Liu, S. Zhang, L. Wang, X. Zheng, L. Zhou, J. Gao, J. Shi, Y. Jiang. Hollow Rh-COF@COF S-Scheme Heterojunction for Photocatalytic Nicotinamide Cofactor Regeneration. *ACS Catal.* **2023**, 13, 6619–6629. DOI: 10.1021/acscatal.2c06332
42. S. S. Zhao, J. Liang, D. -H. Si, M. -J. Mao, Y. B. Huang, R. Cao. Superheterojunction covalent organic frameworks: Supramolecular synergetic charge transfer for highly efficient photocatalytic CO_2 reduction. *Appl. Catal. B Environ. Energy* **2023**, 333, 122782
43. M. Mu, L. Meng, S. Ma, W. Chen, X. Yin, G. Bai. Interfacial imine-bridging and charge directional migration dual regulation of ZnO/covalent organic frameworks S-scheme heterostructure for boosting photocatalytic CO_2 reduction. *J. Colloid Interface Sci.* **2025**, 686, 63–74. DOI: 10.1016/j.jcis.2025.01.232
44. X. Zhu, E. Zhou, X. Tai, H. Zong, J. Yi, Z. Yuan, X. Zhao, P. Huang, H. Xu, Z. Jiang. g-C_3N_4 S-Scheme Homojunction through Van der Waals Interface Regulation by Intrinsic Polymerization Tailoring for Enhanced Photocatalytic H_2 Evolution and CO_2 Reduction. *Angew. Chem. Int. Ed.* **2025**, 64, e202425439. DOI: 10.1002/anie.202425439
45. Z. Wang, C. Bie. HOF/COF 2D/2D S-scheme heterojunction for photocatalytic H_2 production. *J. Mater. Sci. Technol.* **2026**, 243, 206–208. DOI: 10.1016/j.jmst.2025.04.028
46. L. Zhao, C. Bie, B. Cheng. 3D ordered macroporous COF-based S-scheme photocatalyst with enhanced H_2 production. *Chin. J. Struct. Chem.* **2026**, 45, 100834.

47. R. Li, L. Zhang. A van der Waals S-scheme homojunction in g-C3N4. *Chin. J. Catal.* **2026**, 86, 1–4.
48. J. Wang, Y. Yu, J. Cui, X. Li, Y. Zhang, C. Wang, X. Yu, J. Ye. Defective g-C_3N_4/covalent organic framework van der Waals heterojunction toward highly efficient S-scheme CO_2 photoreduction. *Appl. Catal. B Environ. Energy* **2022**, 301, 120814. DOI: 10.1016/j.apcatb.2021.120814
49. Y. Liu, Y. Wang, J. Shang, J. Peng, T. Zhu. Construction of a novel metal-free heterostructure photocatalyst PRGO/TP-COF for enhanced photocatalytic CO_2 reduction. *Appl. Catal. B Environ. Energy* **2024**, 350, 123937. DOI: 10.1016/j.apcatb.2024.123937
50. X. An, J. Bian, K. Zhu, R. Liu, H. Liu, J. Qu. Facet-dependent activity of TiO_2/covalent organic framework S-scheme heterostructures for CO_2 photoreduction. *Chem. Eng. J.* **2022**, 442, 135279. DOI: 10.1016/j.cej.2022.135279
51. J. Cheng, W. Wang, J. Zhang, Z. Liu, S. Wan, B. Cheng, G. Luo, J. Yu, J. Xu, S. Cao. Confining Quantum Dots Within Covalent Organic Framework Cages for Coupled CO_2 Photoreduction and Value-Added Chemical Synthesis. *Adv. Mater.* **2025**, 37, e12144. DOI: 10.1002/adma.202512144
52. P. Dong, A. Zhang, T. Cheng, J. Pan, J. Song, L. Zhang, R. Guan, X. Xi, J. Zhang. 2D/2D S-scheme heterojunction with a covalent organic framework and g-C_3N_4 nanosheets for highly efficient photocatalytic H_2 evolution. *Chin. J. Catal.* **2022**, 43, 2592–2605. DOI: 10.1016/S1872-2067(22)64094-4
53. Y. Zhang, J. Qiu, B. Zhu, M. V. Fedin, B. Cheng, J. Yu, L. Zhang. ZnO/COF S-scheme heterojunction for improved photocatalytic H_2O_2 production performance. *Chem. Eng. J.* **2022**, 444, 136584. DOI: 10.1016/j.cej.2022.136584
54. G. Sun, J. Zhang, B. Cheng, H. Yu, J. Yu, J. Xu. Bifunctional CdS/COF S-scheme photocatalyst for enhanced H_2 evolution and organic synthesis. *Chem. Eng. J.* **2023**, 476, 146818. DOI: 10.1016/j.cej.2023.146818
55. Y. Zhao, C. Yang, S. Zhang, G. Sun, B. Zhu, L. Wang, J. Zhang. Investigating the charge transfer mechanism of ZnSe QD/COF S-scheme photocatalyst for H_2O_2 production by using femtosecond transient absorption spectroscopy. *Chin. J. Catal.* **2024**, 63, 258–269. DOI: 10.1016/S1872-2067(24)60069-0
56. J. Lu, W. Qi, S. Gu, Y. Wang, J. Yu, G. Zhou. Dual Metal-Bridged 2D COF for High Performance of H2O2 Photosynthesis Across Wide pH Range Activated by Dual Route Linkage. *Angew. Chem. Int. Ed.* **2026**, 65, e9931408. DOI: 10.1002/anie.9931408
57. G. Tang, J. Zhang, G. Liang, J. Zhang, C. Bie, J. Yu, H. García. Activating Triplet Excitons in COFs via Layer-Bridging Co Single Atoms for Photocatalytic H_2O_2 Production and Tandem C─N Coupling. *Angew. Chem. Int. Ed.* **2026**, 65, e1580812
58. K. Meng, J. Zhang, B. Zhu, C. Jiang, H. García, J. Yu. Interfacial Charge Transfer in ZnO/COF S-Scheme Photocatalyst via Zn─N Bond. *Adv. Mater.* **2025**, 37, 2505088
59. X. Zhou, C. Bie, X. Wang, Z. Wu, Y. Huo, J. Zhang, J. Yu. N–W bond mediated ultrafast interfacial electron transfer in WO_3/COF S-scheme heterojunction and H_2O_2 photosynthesis mechanism. *Appl. Catal. B Environ. Energy* **2026**, 397, 126930. DOI: 10.1016/j.apcatb.2026.126930
60. X. Wang, F. Zhao, W. Mei, J. Zhang, C. Bie, J. Yu, H. García, F. Xu. Cooperative interfacial preconditioning in an S-scheme heterojunction for CO_2 photoreduction. *Chin. J. Catal.* **2026**, 90, 169–183
61. G. Tang, J. Zhang, C. Bie, X. Zheng, C. Jiang, J. Yu. In Situ Soft X-Ray Absorption Spectroscopy Investigation on Charge Transfer Mechanism in COF/CdS S-Scheme Photocatalyst. *Adv. Mater.* **2025**, 37, e14576. DOI: 10.1002/adma.202514576
62. S. Farhan, W. Fu, M. Humayun, B. Zhu, Y. Wu. Molecular charge bridges drive strong-field S-scheme photocatalysis. *Appl. Catal. B Environ. Energy* **2026**, 395, 126862. DOI: 10.1016/j.apcatb.2026.126862
63. J. Sun, H. Liu, S. Wang, Y. Zhang, C. Bie, L. Zhang. In situ irradiated XPS investigation on S-scheme $ZnIn_2S_4$@COF-5 photocatalyst for enhanced photocatalytic degradation of RhB. *J. Materiomics* **2025**, 11, 100975. DOI: 10.1016/j.jmat.2024.100975
64. Y. Zhao, Y. Zhang, H. Tan, C. Ai, J. Zhang. Rapid charge transfer in TiO_2/COF S-scheme heterojunction for boosting H_2O_2 photosynthesis and Rhodamine B degradation. *J. Materiomics* **2025**, 11, 100970. DOI: 10.1016/j.jmat.2024.100970
65. Y. Liu, M. Li, T. Liu, Z. Wu, L. Zhang. Enhanced charge carrier transport in TiO_2/COF S-scheme heterojunction for efficient photocatalytic H_2O_2 production. *J. Mater. Sci. Technol.* **2025**, 233, 201–209. DOI: 10.1016/j.jmst.2025.03.005
66. Y. Zhang, Y. Wang, Y. Liu, S. Zhang, Y. Zhao, J. Zhang. $MgIn_2S_4$/COF S-scheme heterostructure for improved photocatalytic H_2O_2 production under pure water and air. *J. Materiomics* **2025**, 11, 100985. DOI: 10.1016/j.jmat.2024.100985
67. J. Zhang, S. Li, H. Wu, Y. Peng, Y. Li, P. Deng, L. Zhang, Y. Hou. Efficient separation of charge carriers in the C–S bonded COF@Co_9S_8 S-scheme heterostructure for enhancing the photocatalytic H_2 and H_2O_2 production. *Int. J. Hydrogen Energy* **2025**, 130, 33–44. DOI: 10.1016/j.ijhydene.2025.04.350
68. C. Sun, Z. Fu, Y. Ha, X. Yin, M. Mu. Covalent APTES-Cu_2O/COF hybrid for enhancing CO_2 reduction via S-scheme charge migration. *Colloids Surf. A* **2026**, 742, 140382. DOI: 10.1016/j.colsurfa.2026.140382
69. Z. Zhong, C. Zhou, M. Zhu, H. Yang, Y. Wan, Z. Pan, Q. Cheng. Sb_2S_3@carboxyl-modified COF S-scheme heterojunctions: the Sb–O–C interface enhances photocatalytic CO_2 reduction performance. *Green Chem.* **2026**, 28, 1647–1664. DOI: 10.1039/D5GC04211A
70. H. Jiang, J. Li, X. Yu, H. Dong, W. Wang, Q. Liu. Interface engineering of covalent β-ketoenamine-bridged S-scheme heterojunction for synergistic solar-powered CO_2-to-CO conversion paired with selective alcohol oxidation. *Chin. J. Catal.* **2026**, 80, 113–122. DOI: 10.1016/S1872-2067(25)64883-2
71. X. Xu, S. Dong, J. Lv, G. Huang, Q. Chen, J. Bi. Interfacial C-N-S bridged SnS_2/COF S-scheme heterojunction with upgraded near-infrared photo-activity for H_2O_2 synthesis. *Appl. Surf. Sci.* **2025**, 689, 162489. DOI: 10.1016/j.apsusc.2025.162489
72. H. Wang, F. Zhou, Z. Dai, S. Wei, Y. Wang, Y. Cao, M. Li, J. Li, J. Huang. Rational Construction of Donor–Acceptor Covalent Organic Framework Heterojunction for High-Performance Photocatalytic Production of H_2O_2. *Ind. Eng. Chem. Res.* **2025**, 64, 13211–13220. DOI: 10.1021/acs.iecr.5c01807
73. Z. Tong, D. -K. Ma, J. Wu, X. Hu, N. Jiang, X. Yang, T. Peng. TpPa-1/{010}-$BiVO_4$ S-scheme heterojunction fabricated on specific crystal facets for highly efficient H_2O_2 artificial photosynthesis. *Chem. Eng. J.* **2024**, 496, 154262
74. T. Li, T. Sun, S. Zhang, J. Jiang. A single-atom COF/CdS S-scheme photocatalyst for COF thickness-dependent CO_2 photoreduction. *Sci. China Mater.* **2026**, 69, 3357–3367. DOI: 10.1007/s40843-025-3859-y
75. P. Dong, T. Cheng, J. -L. Zhang, J. Jiang, L. Zhang, X. Xi, J. Zhang. Fabrication of an Organic/Inorganic Hybrid TpPa-1-COF/$ZnIn_2S_4$ S-Scheme Heterojunction for Boosted Photocatalytic Hydrogen Production. *ACS Appl. Energy Mater.* **2023**, 6, 1103–1115
76. Y. Chen, T. Liang, Y. Lin, W. Peng, Z. Chen, W. Lin, Y. -T. Sham, M. Pan, Q. Chen, G. Huang, J. Bi. Enhanced photocatalytic carbon dioxide reduction over iron tungstate/covalent organic framework heterojunctions by the induced unified adsorption and reduction sites. *J. Colloid Interface Sci.* **2026**, 701, 138770
77. J. Qiu, K. Meng, Y. Zhang, B. Cheng, J. Zhang, L. Wang, J. Yu. COF/In_2S_3 S-Scheme Photocatalyst with Enhanced Light Absorption and H_2O_2-Production Activity and fs-TA Investigation. *Adv. Mater.* **2024**, 36, 2400288. DOI: 10.1002/adma.202400288
78. X. Zhou, Y. Huo, S. Yang, B. He, X. Wang, Z. Wu, J. Zhang. Understanding the effect of pH on protonated COF during photocatalytic H_2O_2 production by femtosecond transient absorption spectroscopy. *Acta Phys. Chim. Sin.* **2025**, 41, 100160. DOI: 10.1016/j.actphy.2025.100160
79. Y. He, P. Hu, J. Zhang, G. Liang, J. Yu, F. Xu. Boosting Artificial Photosynthesis: CO_2 Chemisorption and S-Scheme Charge Separation via Anchoring Inorganic QDs on COFs. *ACS Catal.* **2024**, 14, 1951–1961. DOI: 10.1021/acscatal.4c00026
80. Z. Zhong, C. Zhou, M. Zhu, H. Yang, Y. Wan, Z. Pan, Q. Cheng. High-efficient separation of photogenerated carriers in S-scheme BiOI@TpPa-1 heterojunction for enhanced photocatalytic CO_2 reduction: crystal face engineering and DFT calculations. *Inorg. Chem. Front.* **2025**, 12, 7034–7054. DOI: 10.1039/D5QI01127B
81. M. Zhou, H. Liu, Y. Zhang, Y. Liu, K. Chen. In situ synthesis of an S-scheme COF-5@$CsPbBr_3$ heterojunction for efficient photocatalytic CO_2 reduction. *Nanoscale* **2026**, 18, 5023–5032. DOI: 10.1039/D5NR05117G
82. H. Shi, Z. Li, S. Chen, Y. Yao, L. Wu, R. Shao, C. Sheng, S. Zhong, D. Wang, Y. Zhao, L. Zhao, S. Bai. Facet engineering of MOF supports regulates product selectivity in CO_2 photoreduction by modulating electron and proton supply to COF shells. *Chem. Sci.* **2025**, 16, 17688–17702. DOI: 10.1039/D5SC03122B
83. Z. Fan, Y. Cai, Z. Yang, X. Zhang, R. Shao, S. Zhong, L. Zhao, D. Liu, S. Bai. Integrating CO_2 reduction, H_2O oxidation and H_2 evolution catalysts into a dual S-scheme artificial photosynthetic system for tunable syngas production. *Appl. Catal. B Environ. Energy* **2024**, 351, 123979. DOI: 10.1016/j.apcatb.2024.123979
84. H. Xu, X. Lan, S. K. -M. Lai, T. Zhang, H. Yang, E. C. M. Tse, Y. Chen.

Spatial Cascade Sites in Hierarchical COF-Based Photocatalyst Enable C—C Coupling for Selective CO_2 Photoreduction to Ethylene. *Adv. Mater.* **2026**, 38, e73201
85. F. Zhao, F. Xu, J. Yu. Interfacial stabilization of alkali metal oxides on carbon spheres for high-performance CO_2 chemisorption. *Acta Phys. Chim. Sin.* **2026**, 42, 100234. DOI: 10.1016/j.actphy.2025.100234
86. F. Zhao, B. Zhu, L. Wang, J. Yu. Triethanolamine-modified layered double oxide for efficient CO_2 capture with low regeneration energy. *J. Colloid Interface Sci.* **2024**, 659, 486–494. DOI: 10.1016/j.jcis.2023.12.173
87. Y. He, L. Zheng, W. Mei, J. Zhang, C. Bie, J. Yu, H. García, F. Xu. Unveiling Triazine Functionality in COF-Molecular Hybrids for Efficient CO_2 Photoconversion. *Adv. Funct. Mater.* **2026**, 36, e18330
88. J. Zong, Y. Tang, J. Han, G. Wu, W. Xing. Amorphous-Crystalline FeOOH/COF S-Scheme Heterojunctions: Internal Electric Field-Modulated Charge Dynamics for Efficient CO_2 Conversion. *Langmuir* **2026**, 42, 25856–25866. DOI: 10.1021/acs.langmuir.6c03382
89. L. Fang, L. -W. Bai, D. Wu, H. -T. Che, Y. Jiang, Y. Wang, H. Dong, F. -M. Zhang. S-scheme heterojunction of WO_3/metal-covalent organic frameworks for artificial photosynthetic CO_2 reduction. *Chem. Eng. J.* **2025**, 510, 161820
90. C. Liu, T. Gao, G. Wang, Q. Cheng, K. Wang. Efficient CO_2 Photoreduction into Solar Fuels over MoO_{3-x}/COF S-Scheme Photocatalyst. *Chem. Res. Chin. Univ.* **2025**, 41, 726–733. DOI: 10.1007/s40242-025-5033-9
91. K. Tang, W. Deng, N. Wang, Y. Xia, X. Wu, H. Yang. Triazine-based COF/TiO_2 S-scheme heterojunction with oxygen vacancies for efficient photocatalytic CO_2 reduction. *Chin. J. Catal.* **2026**, 83, 244–257. DOI: 10.1016/S1872-2067(26)64987-X
92. Y. Huo, X. Zhou, F. Zhao, C. Ai, Z. Wu, Z. Chang, B. Zhu. Boosting photocatalytic CO_2 methanation through TiO_2/CdS S-scheme heterojunction and fs-TAS mechanism study. *Acta Phys. Chim. Sin.* **2025**, 41, 100148. DOI: 10.1016/j.actphy.2025.100148
93. N. -N. Zhang, Y. Sun, X. -R. Liu, R. Yin, Y. Wang, S. -Y. Wang, J. -Z. Wei, G. Zhang, H. Dong, F. -M. Zhang. 2D MOF/COF Heterojunction for Efficient Photothermal Synergistic Catalysis of CO_2 Reduction. *Adv. Funct. Mater.* **2026**, 36, e23743
94. D. D. Kruger, M. Cabrero-Antonino, S. Osella, F. Xu, J. Yu, A. Primo, H. García. Surface-State–Regulated Product Distribution in Photothermal CO_2 Hydrogenation Over MXene-Based S-Scheme Catalyst. *Angew. Chem. Int. Ed.* **2026**, 65, e8425918
95. X. Nie, X. Wu. Schottky/S-scheme composite heterojunctions for efficient CO_2 photoreduction. *Acta Phys. Chim. Sin.* **2026**, 42, 100192. DOI: 10.1016/j.actphy.2025.100192
96. M. Li, L. Tian. MXene-based S-scheme catalyst for photothermal CO_2 hydrogenation. *Chin. J. Catal.* **2026**, 88, 1–4.
97. P. Hu, J. Zhang, G. Liang, J. Yu, F. Xu. Nonmetal Plasmon-Induced Carrier Backflow and Prolonged Lifetime for CO_2 Photoreduction. *ACS Catal.* **2024**, 14, 15025–15035. DOI: 10.1021/acscatal.4c04644
98. X. Deng, J. Zhang, K. Qi, G. Liang, F. Xu, J. Yu. Ultrafast electron transfer at the In_2O_3/Nb_2O_5 S-scheme interface for CO_2 photoreduction. *Nat. Commun.* **2024**, 15, 4807. DOI: 10.1038/s41467-024-49004-7
99. K. Qi, B. Cheng, M. Setayeshmehr, A. Z. Moshfegh. Solar-driven CO_2-to-chemical conversion via S-scheme photocatalysis and tandem carbonylation. *Chin. J. Catal.* **2026**, 81, 1–4.